Article

Probing Variable Axial Ligation in Nickel Superoxide Dismutase Utilizing Metallopeptide-Based Models: Insight into the Superoxide Disproportionation Mechanism

Kosh P. Neupane, Kristie Gearty, Ashish Francis, and Jason Shearer

J. Am. Chem. Soc., **2007**, 129 (47), 14605-14618 • DOI: 10.1021/ja0731625

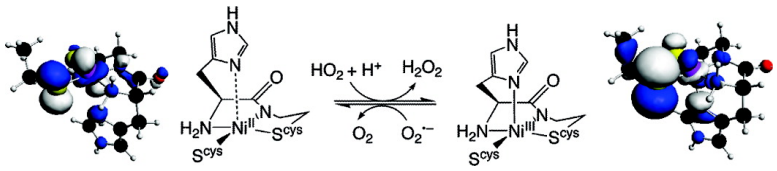

More About This Article

Additional resources and features associated with this article are available within the HTML version:

- Supporting Information
- Links to the 2 articles that cite this article, as of the time of this article download
- Access to high resolution figures
- Links to articles and content related to this article
- Copyright permission to reproduce figures and/or text from this article

View the Full Text HTML

J|A|C|S
ARTICLES
Published on Web 11/07/2007

Probing Variable Axial Ligation in Nickel Superoxide Dismutase Utilizing Metallopeptide-Based Models: Insight into the Superoxide Disproportionation Mechanism

Kosh P. Neupane, Kristie Gearty, Ashish Francis, and Jason Shearer*

Contribution from the Department of Chemistry, University of Nevada, Reno, Reno, Nevada 89557

Received May 4, 2007; E-mail: shearer@unr.edu

Abstract: Nickel superoxide dismutase (NiSOD) is a bacterial metalloenzyme that possesses a mononuclear Ni-center and catalyzes the disproportionation of $O_2^{\bullet-}$ by cycling between Ni^{II} and Ni^{III} oxidation states. Herein we present evidence from several SOD active metallopeptide maquettes ([Ni(SOD^{M2}H(1)X)]; SOD^{M2}H-(1)X = H_2N-XCDLPCG-COOH; X = H, D, or A) that the Ni-center of NiSOD most likely remains five-coordinate during SOD catalysis using thin-film voltammetry. N_3^- and CN^- titration studies suggest that $O_2^{\bullet-}$ disproportionation by [Ni(SOD^{M2}H(1)X)] proceeds via an outersphere mechanism. Computationally derived values for the nuclear reorganization energy of the [Ni^{II}(SOD^{M2})]/[Ni^{III}(SOD^{M2})] self-exchange reaction combined with the experimentally determined value for k_o ($\sim$450 s^{-1}) suggest that axial ligation enhances the $O_2^{\bullet-}$ disproportionation reaction in [Ni(SOD^{M2})] (and NiSOD by analogy) by optimizing the Ni^{II}/Ni^{III} redox couple such that it is close to the midpoint of the $O_2^{\bullet-}$ reduction and oxidation couples.

Superoxide ($O_2^{\bullet-}$) is the product of adventitious O_2 reduction, and is highly toxic to cells if its intracellular concentration reaches into the nanomolar range.[1−5] The reduction of O_2 to $O_2^{\bullet-}$ is unavoidable for aerobic life, thus aerobic organisms have evolved pathways that are capable of degrading $O_2^{\bullet-}$ before it can cause extensive cellular damage. For this purpose most organisms utilize metalloenzymes called superoxide dismutases (SODs),[2,6,7] which disproportionate superoxide into O_2 and H_2O_2 (eq 1).

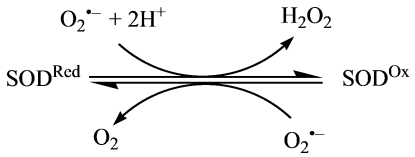

(1)

H_2O_2 can then be degraded through various pathways into harmless products.[8] All known SODs fall into one of four classes based on the transition metal found at their active sites: Cu/Zn-, Fe-, Mn-, and NiSOD.[6−11] NiSOD, the most recently discovered SOD, is found in several cyanobacteria and *Streptomyces* species,[10−12] and exists as a homohexamer in most organisms.[13−14] Each monomer contains one mononuclear Ni-center.

NiSOD disproportionates $O_2^{\bullet-}$ by cycling between the reduced Ni^{II} and oxidized Ni^{III} oxidation states (Figure 1). X-ray crystallography[13,14] has demonstrated that in its reduced Ni^{II} resting state the Ni−center is ligated by two *cis*-cysteinates (from C(2) and C(6)), an amide nitrogen derived from the peptide backbone (from C(2)), and the N-terminal amine-nitrogen (from H1) forming a square planar geometry. Upon oxidation to the Ni^{III} oxidation state, the imidazole from H(1) coordinates to Ni forming a square pyramidal Ni-center. We note that all of the ligands to both Ni^{II} and Ni^{III} are derived from residues between H(1) and C(6), which form a loop about Ni. This region of NiSOD has therefore been termed the Ni-binding hook. Despite the fact that the crystal structures of reduced and oxidized NiSOD have been solved, there are a number of important questions concerning the physical and reactive properties of the metalloenzyme that remain unknown. For example, it is possible that the crystal structures obtained for NiSOD may be relevant only to the metalloenzyme's resting states.

Maroney and co-workers have demonstrated that the axial H(1) imidazole is vitally important in optimizing the rate of

(1) Imlay, J. A. *Annu. Rev. Microbiol.* **2003**, *57*, 395−418.
(2) Valentine, J. S.; Wertz, D. L.; Lyons, T. J.; Liou, L. L.; Goto, J. J.; Gralla, E. B. *Curr. Opin. Chem. Biol.* **1998**, *2*, 253−262.
(3) Miller, A.-F.; Sorkin, D. L. *Comments Mol. Cell. Biophys.* **1997**, *9*, 1−48.
(4) Fridovich, I. *J. Biol. Chem.* **1989**, *264*, 7761−7764.
(5) Kurtz, D. M., Jr. *Acc. Chem. Res.* **2004**, *37*, 902−908.
(6) Fridovich, I. *Annu. Rev. Biochem.* **1995**, *64*, 97−112.
(7) Miller, A.-F. *Curr. Opin. Chem. Biol.* **2004**, *8*, 162−168.
(8) Zamocky, M.; Koller, R. *Prog. Biophys. Mol. Biol.* **1999**, *72*, 19−66.
(9) Fridovich, I. *Encycl. Biol. Chem.* **2004**, *4*, 135−138.
(10) Youn, H.-D.; Kim, E.-J.; Roe, J.-H.; Hah, Y. C.; Kang, S.-O. *Biochem. J.* **1996**, *318*, 889−896.
(11) Youn, H.-D.; Youn, H.; Lee, J.-W.; Yim, Y.-I.; Lee, J. K.; Hah, Y. C.; Kang, S.-O. *Arch. Biochem. Biophys.* **1996**, *334*, 341−348.
(12) Palenik, B.; Brahamsha, B.; Larimer, F. W.; Land, M.; Hauser, L.; Chain, P.; Lamerdin, J.; Regala, W.; Allen, E. E.; McCarren, J.; Paulsen, I.; Dufresne, A.; Partensky, F.; Webb, E. A.; Waterbury, J. *Nature* **2003**, *424*, 1037−1042.
(13) Wuerges, J.; Lee, J.-W.; Yim, Y.-I.; Yim, H.-S.; Kang, S.-O.; Carugo, K. D. *Proc. Natl. Acad. Sci. U.S.A.* **2004**, *101*, 8569−8574.
(14) Barondeau, D. P.; Kassmann, C. J.; Bruns, C. K.; Tainer, J. A.; Getzoff, E. D. *Biochemistry* **2004**, *43*, 8038−8047.

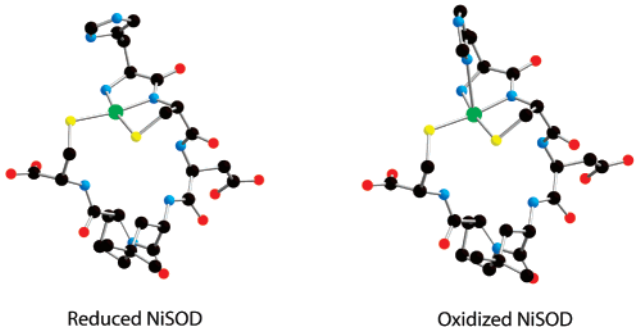

Figure 1. Structures of the reduced and oxidized forms of NiSOD highlighting the Ni binding hook.

$O_2^{\bullet-}$ disproportionation.[15] It was shown that the NiSOD mutant H(1)Q-NiSOD, which appears to effect a positive shift in the enzymes redox potential based on the fact the mutant metalloenzyme is found predominantly in the reduced state, yielded a 2-order of magnitude reduction in the rate of $O_2^{\bullet-}$ disproportionation. This demonstrates the importance of the axial H(1) imidazole in fine-tuning the physical and reactive properties of the metalloenzyme. Furthermore, Maroney's study implied that the axial ligand most likely remains bound to Ni during at least part of the catalytic cycle.

Kinetic studies performed using NiSOD from *S. seoulensis* and *S. coelicolor* show that the metalloenzyme performs superoxide disporportionation near the diffusion limit ($k_{cat} > 2 \times 10^9$ M^{-1} s^{-1}).[15,16] This might appear to be at odds with the large structural rearrangement apparently taking place at the Ni-center during catalysis revealed by the crystal structures of NiSOD (i.e., the imidazole coordinating/uncoordinating). It is therefore possible that the crystal structure of reduced NiSOD is relevant only to the resting state of the metalloenzyme. This was supported by a recent computational study probing the reaction mechanism of NiSOD.[17] In that hybrid density functional theory study by Pelmenschikov and Siegbahn, it was suggested that the lowest energy catalytic pathway for NiSOD is one that involves imidazole coordination to Ni *throughout catalysis*. This proposal helps to reconcile the fast value recorded for k_{cat} with the enzyme's active site structure, but experimental evidence has yet to be presented to support or refute the notion of five-coordinate Ni^{II} during NiSOD catalysis.

Our investigations concerning NiSOD have focused on understanding how the primary coordination sphere contributes to the reactivity and stability of the Ni-center.[18−20] Some of this work has involved the preparation and subsequent investigation of metallopeptide-based NiSOD models.[18,19] The validity of using a metallopeptide-based modeling approach was highlighted using the metalloprotein maquette [Ni^{II}(SOD^{M1})]. [Ni^{II}(SOD^{M1})] is a metallopeptide based on the first twelve residues from the N-terminal sequence of *S. coilicolor* NiSOD (SOD^{M1}: H_2N-HCDLPCGVYDPA).[18] This metallopeptide represents a spectroscopic *and* active synthetic analogue of NiSOD; [Ni^{II}(SOD^{M1})] reproduces the key spectroscopic and structural properties of reduced NiSOD while affording SOD activity approaching that of native SODs.[18,19]

In this study we utilize the maquette [Ni^{II}(SOD^{M2})] (SOD^{M2}: H_2N-HCDLPCG), which is composed only of the residues found within the Ni-binding hook. This peptide is therefore the minimal Ni-binding fragment that is capable of maintaining Ni in a coordination environment and geometry nearly identical to NiSOD. Through the systematic "mutation" of the N-terminal residue of SOD^{M2} (producing SOD^{M2}H(1)X, where X = A or D) the influence that differing axial ligation to Ni has on the redox, spectroscopic, structural, and SOD activity properties of the metallopeptide can be readily probed. These data yield new insight into the active-site structure and mechanism of NiSOD. Specifically, it will be demonstrated that the H1 imidazole in NiSOD most likely remains ligated during catalysis.

Experimental Section

Peptide Synthesis and Metallopeptide Preparation. All peptides were prepared by manual solid-phase peptide synthesis utilizing standard Fmoc/^{t}Bu-based protection strategies on Wang resin with HBTU/HOBt/DIEPA coupling methods.[21] The peptides were cleaved from the resin using a mixture of 95% TFA/2.5% ethanedithiol/2.5% triisopropyl silane and then filtered. The filtrate was then evaporated under vacuum forming a glassy film, which was washed several times with freshly distilled diethyl ether resulting in tan-colored crude peptides. All peptides were then subsequently purified by reverse phase HPLC on a Waters DeltPrep 60 equipped with a Waters Atlantis C-18 reverse phase column (5 μm; 50 mm × 100 mm). A gradient of 10−29% MeCN (0.1% TFA) in H_2O (0.1% TFA) over 15 min was used with a flow rate of 40 mL min^{-1}. The fractions containing the desired product were then lyophilized yielding white powders. The purity of each peptide was assessed by analytical reverse phase HPLC (Atlantis C-18 reverse phase column 5 μm; 4.6 mm × 100 mm; gradient, 10−65% MeCN (0.1% TFA) in H_2O (0.1% TFA) over 45 min; flow rate of 1 mL min^{-1}) and mass spectrometry on a Waters Micromass 20 ESI mass spectrometer (negative ion mode).

SOD^{M2} (H_2N-HCDLPCG). R_t = 10.8 min (analytical); 3.7 min (preparative). Yield = 76%. ESI-MS (neg. ion) M^- *m/z* calcd 742.8; found, 742.4.

SOD^{M2}H(1)A (H_2N-ACDLPCG). R_t = 15.4 min (analytical); 3.8 min (preparative). Yield = 61%. ESI-MS (neg. ion) M^- *m/z* calcd 676.8; found, 677.8.

SOD^{M2}H(1)D (H_2N-DCDLPCG). R_t = 14.6 min (analytical); 3.8 min (preparative). Yield = 53%. ESI-MS (neg. ion) M^- *m/z* calcd 720.8; found, 720.2.

Metalated [Ni^{II}(SOD^{M2})] and [Ni^{II}(SOD^{M2}H(1)X)] were prepared by adding 1 equiv of $NiCl_2$ to 1 equiv of the apo-peptide in 50 mM *N*-ethylmorpholine (NEM) buffer (pH = 7.5). Peptide concentrations were quantified by the procedure of Ellman.[22] Ni^{II} was added to solution as $NiCl_2$ in neutral water and the pH of the metallopeptide solution adjusted to 7.4. Gel permeation chromatography studies were performed on a Waters DeltPrep 60 equipped with a Protein-Pak GPC column (7.8 mm × 300 mm; 60 Å pore size) using an aqueous solution of $NaHCO_3$ (saturated) under a positive pressure of He flowing at 1 mL min^{-1}. Data were recorded at 350 nm where the free peptides do not significantly absorb. Calibration curves were made using a Waters polyethylene glycol standard kit.

(15) Bryngelson, P. A.; Arobo, S. E.; Pinkham, J. L.; Cabelli, D. E.; Maroney, M. J. *J. Am. Chem. Soc.* **2004**, *126*, 460−461.
(16) Choudhury, S. B.; Lee, J.-W.; Davidson, G.; Yim, Y.-I.; Bose, K.; Sharma, M. L.; Kang, S.-O.; Cabelli, D. E.; Maroney, M. J. *Biochemistry* **1999**, *38*, 3744−3752.
(17) Pelmenschikov, V.; Siegbahn, P. E. M. *J. Am. Chem. Soc.* **2006**, *128*, 7466−7475.
(18) Shearer, J.; Long, L. M. *Inorg. Chem.* **2006**, *45*, 2358−2360.
(19) Neupane, K. P.; Shearer, J. *Inorg. Chem.* **2006**, *45*, 10552−10566.
(20) Shearer, J.; Zhao, N. *Inorg. Chem.* **2006**, *45*, 9637−9639.

(21) Abbreviations: HOBt, 1-hydroxybenotriazole; HBTU, *N*-[(1*H*-benzotriazol-1-yl)(dimethylamino)methylene]-*N*-methylmethanaminium hexaflurophosphate *N*-oxide; DIPEA, *N*,*N*-diisopropylethylamine.
(22) Ellman, G. L. *Arch. Biochem. Biophys.* **1958**, *74*, 443−450.

[Ni^{II}(SOD^{M2})]. Electronic absorption spectrum λ_{max} nm (ϵ M^{-1} cm^{-1}): 616 (sh), 561(sh), 457 (345), 352 (sh). ESI-MS (neg. ion) M$^-$ *m*/*z* calcd 798.7; found, 798.5.

[Ni^{II}(SOD^{M2}H(1)A)]. Electronic absorption spectrum λ_{max} nm (ϵ M^{-1} cm^{-1}): 964 (25), 704 (sh), 543 (sh), 458 (427). ESI-MS (neg. ion) M$^-$ *m*/*z* calcd 732.7; found, 732.1.

[Ni^{II}(SOD^{M2}H(1)D)]. Electronic absorption spectrum λ_{max} nm (ϵ M^{-1} cm^{-1}): 977 (20), 693 (sh), 538(sh), 461 (327). ESI-MS (neg. ion) M$^-$ *m*/*z* calcd 755.8; found, 755.6.

Electronic Absorption and CD Measurements and SOD Activity and Inhibitor Binding Studies. All solutions were prepared from water that had an initial resistance of at least 18 MΩ. Electronic absorption measurements were carried out on either a Varian Cary-50 or an OLIS−CARY 14 UV-vis-NIR spectrophotometer using quartz cuvettes with 1 cm pathlengths. CD spectroscopic measurements were performed on an OLIS DSM 17 CD spectropolarimeter using cuvetts with a 1 cm path length. All spectra were obtained in 50 mM NEM (pH 7.4). SOD activity assays were performed at pH 7.4 utilizing the modified xanthine/xanthine oxidase assay of Tabbi et al. as previously described.[23] In addition, an NBT/formazan assay was performed as follows.[18] A solution of 0.030 mM NBT in 50 mM NEM (pH 7.4) was prepared. To this 0.010 mM [Ni^{II}(SOD^{M2}H(1)X)] was added. KO_2 (in DMSO for concentrations <100 equiv and solid KO_2 for higher concentrations) was then added to these solutions, resulting in the formation of formazan ($\epsilon_{560} \approx 35{,}000$ M^{-1} cm^{-1}). Blank and control experiments were run with either no metallopeptide added, or 0.010 mM $NiCl_2$ or apo-peptide added. In the case of the blank and control experiment 50 equiv of KO_2 (per NBT) had to be added to solution to afford the complete conversion of NBT to formazan. To screen for CN^- or N_3^- binding to the Ni-center of [Ni^{II}(SOD^{M2})] a pH 7.4 solution (50 mM NEM) of NaCN or NaN_3 was added to a 1.5 mM solution of [Ni^{II}(SOD^{M2})] (pH 7.4; 50 mM NEM). The influence that addition of NaCN or NaN_3 had on the electronic absorption spectrum of [Ni^{II}(SOD^{M2})] was examined. Up to 300 equiv of NaCN or NaN_3 was added to solution in either 1 or 10 equiv increments.

Determination of Ni^{II} Stability Constants for [Ni^{II}(SOD^{M2})] and [Ni^{II}(SOD^{M2}H(1)X)]. Stability constants for the metallopeptides were determined spectrophotometrically on a CARY-50 UV−vis−NIR spectrophotometer. All studies were performed at pH = 7.4 (50 mM NEM buffer) using glycine as a competitive Ni^{II} chelate. In a typical experiment a solution of glycine (pH = 7.4) was titrated into a solution of [Ni^{II}(SOD^{M2})] or [Ni^{II}(SOD^{M2}H(1)X)], causing Ni^{II} to be extracted from the metallopeptide. The concentration of all species present were then calculated using the methods of Drago and co-workers to deconvolute the concentrations of [Ni^{II}(SOD^{M2})H(1)X] and [Ni^{II}(gly)$_2$] from the electronic absorption data.[24,25] The following wavelengths were utilized for analyzing the titration results: [Ni^{II}(SOD^{M2})] 454 nm (ϵ = 345 M^{-1} cm^{-1}); [Ni^{II}(SOD^{M2}H(1)A)] 458 nm (ϵ = 427 M^{-1} cm^{-1}); [Ni^{II}(SOD^{M2}H(1)D)] 461 nm (ϵ = 342 M^{-1} cm^{-1}). Once the concentration of all species present at a given glycine concentration were determined, the dissociation constant (K_d) for [Ni^{II}(SOD^{M2})] or [Ni^{II}(SOD^{M2}H(1)X)] was calculated according to

$$K_d = \beta^{-1} K_{ex}^{-1} \tag{2}$$

where

$$K_{ex}^{-1} = \frac{[Ni^{II}(gly)_2][SOD^{M2}H(1)X]}{[Ni^{II}(SOD^{M2}H(1)X)][gly]^2} \tag{3}$$

and the value for β for glycine at pH 7.4 is 5.01×10^5 M^{-1}.[26] The reported K_d values represent the average of three trials.

X-ray Absorption Spectroscopy Data Measurement and Analysis. Freshly prepared samples of [Ni^{II}(SOD^{M2})H(1)X] (~1.5 mM, pH 7.4, 50 mM NEM) were injected into an aluminum sample holder between windows made from Kapton tape (3M, Minneapolis, MN; cat. no. 1205) and quickly frozen in liquid nitrogen. Data were collected at the National Synchrotron Light Source, Brookhaven National Laboratories (Upton, NY) on beamlines X9b and X3b. The samples were maintained at 20 K throughout data collection using a He Displex cryostat. All spectra are reported as fluorescence data and recorded on a Canberra 13-element solid-state Ge fluorescence detector. Total count rates were maintained under 30 kHz per channel, and each channel was individually inspected for data quality prior to data averaging. For the edge spectra the primary hutch aperture was set to 0.4 mm to obtain the maximum spectral resolution, and data were collected in 10 eV steps in the pre-edge region (8131−8310 eV), 0.3 eV steps in the edge region (8310−8350 eV) and 2.0 eV steps in the near edge region. EXAFS data collection utilized a primary hutch aperture height of 0.8 mm and data were collected in 10 eV steps in the pre-edge region (8131−8310 eV), 0.5 eV steps in the edge region (8310−8350 eV), 2.0 eV steps in the near edge region (8352−8630 eV), and 5.0 eV steps in the far-edge region (8631 eV−5.5 k). The spectra reported represent the average of at least four data sets. Data analysis were performed using the XAS refinement and graphing package EXAFS123 provided by Prof. R. C. Scarrow (Haverford College; Haverford, PA).[27] We present refinements based on unfiltered k^3 weighted data performed in an analogous manner as previously described.[18,19] EXAFS data were then analyzed to 14.3 k owing to noise at higher energies. The goodness of fit was judged using

$$\epsilon^2 = [n_{idp}/(n_{idp} - n_p)] \times \text{average}[(y_{data} - y_{model})/\sigma]^2 \tag{4}$$

where n_{idp} is the number of independent data points, n_p is the number of refined parameters, σ is the estimated uncertainty in the data, y_{data} is the experimental k^3 EXAFS spectrum, and y_{model} is the simulated k^3 EXAFS spectrum.

Electron Paramagnetic Resonance Experiments. [Ni^{III}(SOD^{M2})] was generated in a 1:1 mixture of buffer solution:glycerol (buffer solution: 50 mM NEM pH 7.4) in a quartz EPR tube. In a typical experiment 0.9 equiv of KO_2 (in DMSO) was added to a 0.050 mM solution of [Ni^{II}(SOD^{M2})]. This was quickly mixed in a vortex mixer and immediately frozen in liquid nitrogen. The EPR spectrum was recorded in a quartz finger dewar in liquid nitrogen on a Varian E4 EPR spectrometer interfaced to a personal computer through a Scientific Software Services EWWIN system. Data were averaged over 20 scans.

Electrochemical Measurements. Electrochemical measurements were performed on a Princeton Applied Research PARSTAT 2273 potentiostat in a Faraday cage to minimize noise in the voltammograms. We utilized a glass cell with a solution containing the metallopeptide (1.0 mM) and $NaClO_4$ (100 mM) buffered to pH = 7.4 (10 mM NEM buffer). The solutions were continually sparged with Ar prior to data collection and maintained under a positive pressure of Ar during data collection. We utilized a standard three electrode cell with a Ag/AgCl reference electrode, a Pt wire auxiliary electrode, and a glassy carbon disk working electrode (A = 0.2 cm^2). Cyclic voltammograms were recorded for these solutions at a scan velocity of 100 mV s^{-1}. Thin films of [Ni^{II}(SOD^{M2})] and [Ni^{II}(SOD^{M2}H(1)A)] were prepared according to the procedure of Rusling et al.[28] Briefly, a 10 mM solution of *N*,*N*-dimethyldidodecylammonium bromide (DDAB) was prepared by sonicating a water suspension of the appropriate mass of insoluble DDAB for 4 h by which time the solution had become clear. A 0.5 mM solution (1 mL) of the metallopeptide was then added to 1 mL of the DDAB solution. A 10 μL portion of the solution was then applied to a pyrolytic graphite electrode ($A \approx 0.02$ cm^2),[29] which was polished with 1 μm alumina and then sonicated prior to use. The DDAB/

(23) Tabbi, G.; Driessen, W. L.; Reedijk, J.; Bonomo, R. P.; Veldman, N.; Spek, A. L. *Inorg. Chem.* **1997**, *36*, 1168−1175.
(24) Gidry, R. M.; Drago, R. S. *J. Am. Chem. Soc.* **1973**, *95*, 6645−6648.
(25) Epley, T. D.; Drago, R. S. *J. Am. Chem. Soc.* **1969**, *91*, 2883−2890.
(26) Dawson, R. M. C.; Elliot, D. C.; Elliot, W. H.; Jones, K. M. *Data for Biochemical Research*, Claredon Press: Oxford, U.K., 1986.
(27) Scarrow, R. C. *EXAFS123*, Haverford College: Haverford, PA, 2005.
(28) Rusling, J. F.; Nassar, A.-E. F. *J. Am. Chem. Soc.* **1993**, *115*, 11891−11897.

metallopeptide solution was allowed to evaporate, and the electrode was secured in the cell. The reference electrode was positioned such that the capillary tip housing the Ag/AgCl reference electrode was normal to the working electrode at a distance ~1 mm from the working electrode's surface. A piece of Pt wire was used for the auxiliary electrode. Cyclic voltammograms were collected for these metallopeptide films over scan rates of (0.005−50 V s^{-1}). The background current was subtracted from the data by fitting a cubic spline function to the baseline on each side of the peak. Numerical modeling of the waveforms was then accomplished as previously described using the finite difference procedure with 0.1 mV step sizes.[29−32]

Electronic Structure Calculations. Geometry optimization (GO) and frequency calculations were performed using the Amsterdam density functional (ADF) software package version 2005.01.[33] We used the ADF default convergence criteria for all calculations. Initial coordinates were imported from the crystal structures of reduced ($(Ni^{II}(SOD\text{-}off))^-$) and oxidized ($Ni^{III}(SOD\text{-}on)$) nickel superoxide dismutase.[14] Hydrogen atoms were then placed in idealized geometries prior to the geometry optimization. The frozen-core approximation was used for the 1s orbital of all second row elements and the 1s, 2s, and 2p orbitals for Ni and S. The valance orbitals were treated utilizing the ADF TZDP basis set (triple-ζ basis set with double polarization). Calculations were performed using the local density approximation of Vosko, Wilk, and Nussair[34] and the nonlocal gradient corrections of Beck[35−37] and Perdew.[38,39] To obtain the GO structure for imidazole unbound oxidized $Ni^{III}(SOD\text{-}off)$, the coordinates from the GO structure of $(Ni^{II}(SOD\text{-}off))^-$ was used as the initial atomic coordinates for $Ni^{III}(SOD\text{-}off)$, and then the geometry optimization was performed. Similarly, GO structured of low- ($(Ni^{II}(SOD\text{-}on^{l.s.}))^-$) and high-spin ($(Ni^{II}(SOD\text{-}on^{h.s.}))^-$) $(Ni^{II}(SOD\text{-}on))^-$ were obtained using the GO structure of $Ni^{III}(SOD\text{-}on)$ for the initial atomic coordinates followed by the geometry optimization on the reduced metallopeptides. Atomic orbital contributions to the corresponding molecular orbitals are reported as Mulliken populations.

Inner-sphere reorganization energies (λ_i) for the self-exchange reactions

$$(Ni^{II}(SOD\text{-}off))^- + Ni^{III}(SOD\text{-}on) \rightleftharpoons Ni^{III}(SOD\text{-}on) + (Ni^{II}(SOD\text{-}off))^- \quad (5)$$

$$(Ni^{II}(SOD\text{-}off))^- + Ni^{III}(SOD\text{-}on) \rightleftharpoons Ni^{III}(SOD\text{-}off) + (Ni^{II}(SOD\text{-}off))^- \quad (6)$$

$$(Ni^{II}(SOD\text{-}on^{l.s.}))^- + Ni^{III}(SOD\text{-}on) \rightleftharpoons Ni^{III}(SOD\text{-}on) + (Ni^{II}(SOD\text{-}on^{l.s.}))^- \quad (7)$$

$$(Ni^{II}(SOD\text{-}off^{h.s.}))^- + Ni^{III}(SOD\text{-}on) \rightleftharpoons Ni^{III}(SOD\text{-}on) + (Ni^{II}(SOD\text{-}on^{h.s.}))^- \quad (8)$$

were subsequently calculated using the methods of Jakobsen et al.[40] In reactions 5−8 the on and off represent ligated and unligated imidazole ligands, respectively. We will briefly describe the process for calculating λ_i using eq 5 as an example. GO structures for $(Ni^{II}(SOD\text{-}off))^-$ and $Ni^{III}(SOD\text{-}off)$ were calculated along with their force constant matrices **F**. A projected force constant f is obtained for $(Ni^{II}(SOD\text{-}off))^-$ (f_r) and $Ni^{III}(SOD\text{-}off)$ (f_o) by applying

$$f = \frac{\Delta\mathbf{q}^T\mathbf{F}\Delta\mathbf{q}}{|\Delta\mathbf{q}|^2} \quad (9)$$

where $|\Delta\mathbf{q}|$ is the norm of the vector $\Delta\mathbf{q}$, which describes the atomic displacement of all of the atoms from the idealized (GO) structure of the reduced (or oxidized) species to the oxidized (or reduced) species, and $\Delta\mathbf{q}^T$ is the transpose of vector $\Delta\mathbf{q}$. From the projected force constant the innersphere reorganization energy λ_i can be calculated by

$$\lambda_i = \frac{f_r f_o}{(f_r + f_o)}|\Delta\mathbf{q}|^2 \quad (10)$$

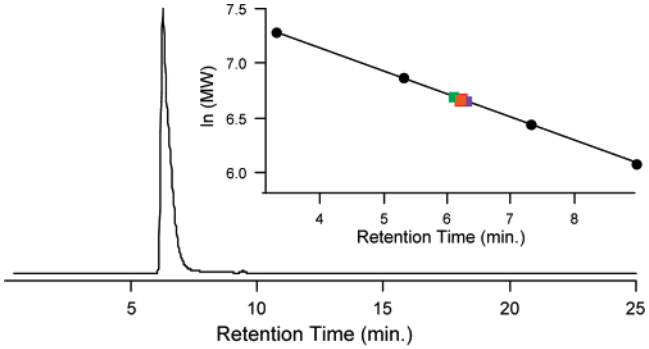

Figure 2. Gel permeation chromatogram of $[Ni^{II}(SOD^{M2})]$ obtained at a wavelength of 350 nm under a positive pressure of He. The mobile phase is a saturated $NaHCO_3$ solution (pH = 8.4). The inset depicts where $[Ni^{II}(SOD^{M2})]$ (orange square), $[Ni^{II}(SOD^{M2}H(1)A)]$ (purple square), and $[Ni^{II}(SOD^{M2}H(1)D)]$ (green square) fall on the calibration curve (black circles and line).

Results and Discussion

Preparation of $SOD^{M2}H(1)X$ and Subsequent Metalation With Ni^{II}. The peptide SOD^{M2} (H_2N-HCDLPCG) was prepared in good yields (76%) by standard Fmoc-based solid-phase synthesis followed by purification using preparative HPLC and lyophilization. The anaerobic addition of 1 equiv of $NiCl_2$ to solutions of SOD^{M2} (pH 7.4, 50 mM NEM) caused the colorless solution to turn to a pink/beige color, similar to what is observed with $[Ni^{II}(SOD^{M1})]$. SOD^{M2} will only coordinate 1 equiv of Ni^{II} per peptide as assessed by ESI-MS (m/z = 797.1). Gel permeation chromatography (GPC) indicates that $[Ni^{II}(SOD^{M2})]$ is monomeric in solution (Figure 2). All GPC data were collected at a wavelength of 350 nm such that only the metallopeptide, and not the free peptide, was observed. Chromatograms recorded at 254 nm were identical to those obtained at 350 nm indicating there is minimal apo-peptide present in solution. The apparent molecular weight of $[Ni^{II}(SOD^{M2})]$ obtained by GPC is 790 Da, which compares well with the ESI-MS data.[41]

The Ni^{II} dissociation constant (K_d) for $[Ni^{II}(SOD^{M2})]$ was determine spectrophotometrically using glycine as a competitive Ni^{II} chelate (Figure 3, Table 1). By applying eqs 2 and 3 a K_d = 5(1) μM was obtained for $[Ni^{II}(SOD^{M2})]$. This is similar to the $K_d \approx 1$ μM obtained for $[Ni^{II}(SOD^{M1})]$.[19] Thus, these data

(29) Jeuken, L. J. C.; Armstrong, F. A. *J. Phys. Chem. B* **2001**, *22*, 5271−5282.
(30) Britz, D. *Digital Simulations in Electrochemistry*; Springer-Verlag: Berlin, 2006; Vol. 3.
(31) Hirst, J.; Armstrong, F. A. *Anal. Chem.* **1998**, *70*, 5062−5071.
(32) Hirst, J.; Duff, J. L. C.; Jameson, G. N. L.; Kemper, M. A.; Burgess, B. K.; Armstrong, F. A. *J. Am. Chem. Soc.* **1998**, *120*, 7085−7094.
(33) Te Velde, G.; Bickelhaupt, F. M.; Baerends, E. J.; Guerra, C. F.; Van Gisbergen, S. J. A.; Snijders, J. G.; Ziegler, T. *J. Comp. Chem.* **2001**, *22*, 931−967.
(34) Vosko, S. J.; Wilk, M.; Nussair, M. *Can. J. Phys.* **1980**, *58*, 1200−1211.
(35) Becke, A. *J. Chem. Phys.* **1986**, *84*, 4524−4529.
(36) Becke, A. *J. Chem. Phys.* **1988**, *88*, 1053−1062.
(37) Becke, A. *Phys. Rev. A* **1988**, *38*, 3098−3100.
(38) Perdew, J. P. *Phys. Rev. B* **1986**, *34*, 7406.
(39) Perdew, J. P. *Phys. Rev. B* **1986**, *33*, 8822−8824.
(40) Jakobsen, S.; Mikkelsen, K. V.; Pedersen, S. U. *J. Phys. Chem.* **1996**, *100*, 7411−7417.

(41) There is at least a 30% error associated with the experimentally derived mass from GPC.

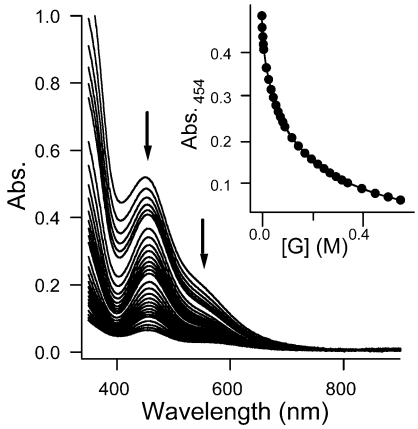

Figure 3. Representative glycine titration study performed on [$Ni^{II}(SOD^{M2})$] (50 mM NEM, pH 7.4). The inset displays the change in absorbance at 454 nm as a function of glycine concentration with a trend line connecting the data points.

indicate that the removal of the five residues outside of the Ni-binding hook is not significantly compromising the Ni^{II} affinity of the metallopeptide.

A major goal of this study is to probe how altering the N-terminal residue will influence the properties of the resulting NiSOD metallopeptide based mimics. Therefore, in addition to SOD^{M2} the peptides SOD^{M2}H(1)A (alanine in place of H(1)) and SOD^{M2}H(1)D (aspartic acid in place of H(1)) were prepared in moderate to good yields (50 − 60%) through solid-phase peptide synthesis. Metalation of these peptides in anaerobic buffer (50 mM NEM pH 7.4) also produced lightly colored pink-beige solutions. Similar to SOD^{M2} these two peptides will coordinate 1 equiv of Ni^{II} (as assessed by ESI-MS) and are monomeric in solution (as assessed by GPC, Figure 1). The K_d values obtained for [$Ni^{II}(SOD^{M2}H(1)X)$] are 6(3) μM for [Ni^{II}-(SOD^{M2}H(1)A)] and 7(3) μM for [$Ni^{II}(SOD^{M2}H(1)D)$] (Table 1). The similarity in Ni^{II} dissociation constants seems to indicate that similar Ni-binding modes exist in solution for the three metallopeptides prepared.

Spectroscopic, Structural, and Redox Properties of [Ni^{II}-(SOD^{M2})H(1)X]. The pH 7.4 (50 mM NEM) electronic absorption and CD spectra of [$Ni^{II}(SOD^{M2})$], [$Ni^{II}(SOD^{M2}H(1)A)$], and [$Ni^{II}(SOD^{M2}H(1)D)$] are displayed in Figure 4. The spectra obtained for [$Ni^{II}(SOD^{M2})$] compare well with those obtained for the longer NiSOD metallopeptide mimic [$Ni^{II}(SOD^{M1})$]. [$Ni^{II}(SOD^{M2})$] displays a well-defined peak at 21 900 cm^{-1} (457 nm, $\epsilon = 345\ M^{-1}\ cm^{-1}$) in the electronic absorption spectrum. Previous studies by us and others have identified that this band is mostly composed of a Ni($3d_{xy}$)/S(π)* → Ni($3d_{x^2-y^2}$/S/N(σ))* transition.[19,20,42] This band is a characteristic feature in square-planar $Ni^{II}N_2S_2$ complexes, and differences in the energy of this feature from one structurally related $Ni^{II}N_2S_2$ to another can be correlated to a destabilization of the Ni($3d_{x^2-y^2}$/S/N(σ))* LUMO (i.e., an increase in $10D_q$).[20] The corresponding feature in [Ni^{II}-(SOD^{M1})] occurs at 21 800 cm^{-1} (458 nm), which is nearly identical to that obtained for [$Ni^{II}(SOD^{M2})$].[18] This indicates that the elimination of the nonbonding residues outside of the Ni-binding hook is not having a major impact on the electronic structure of the Ni^{II}-center of the shorter metallopeptide. Other features in the electronic absorption spectrum of [$Ni^{II}(SOD^{M2})$] also correspond well with those reported for [$Ni^{II}(SOD^{M1})$]. These include the shoulder at 18 250 cm^{-1} (548 nm, $\epsilon = 130\ M^{-1}\ cm^{-1}$), corresponding to the feature at 18 100 cm^{-1} (552 nm) for [$Ni^{II}(SOD^{M1})$]; the low-energy feature at 12 150 cm^{-1} (823 nm, $\epsilon = 50\ M^{-1}\ cm^{-1}$), corresponding to the feature at 11 850 cm^{-1} (843 nm) for [$Ni^{II}(SOD^{M1})$]; and the high-energy feature at 27 625 cm^{-1} (361 nm, $\epsilon = 656\ M^{-1}\ cm^{-1}$), corresponding to the feature at 29 700 cm^{-1} (337 nm) for [Ni^{II}-(SOD^{M1})].

The CD spectrum of [$Ni^{II}(SOD^{M2})$] also compares well with that reported for [$Ni^{II}(SOD^{M1})$].[18,19] The most prominent features in the CD spectra of the two metallopeptides are the negative signed features at 22 220 cm^{-1} ($\Delta\epsilon = -1.5\ M^{-1}\ cm^{-1}$) in [$Ni^{II}$-($SOD^{M2}$)] versus 21 830 cm^{-1} in [$Ni^{II}(SOD^{M1})$]. This 370 cm^{-1} shift in energy is considerably less than the 2150 cm^{-1} shift in the energy of this feature upon acylation of the N-terminus of [$Ni^{II}(SOD^{M1})$] (forming a bis-amide $Ni^{II}N_2S_2$ coordination environment), indicating similar coordination environments in [$Ni^{II}(SOD^{M1})$] versus [$Ni^{II}(SOD^{M2})$]. Other features in the CD spectrum of [$Ni^{II}(SOD^{M2})$] also compare well with those obtained for [$Ni^{II}(SOD^{M1})$] including the low-energy positive signed feature at 11 400 cm^{-1} ($\Delta\epsilon_{max} = 0.9\ M^{-1}\ cm^{-1}$ vs 11 200 cm^{-1} for [$Ni^{II}(SOD^{M1})$]), the negative signed feature at 14 190 cm^{-1} ($\Delta\epsilon_{max} = -0.4\ M^{-1}\ cm^{-1}$ vs 13 700 cm^{-1} for [Ni^{II}-(SOD^{M1})]), the positive signed feature at 17 625 cm^{-1} ($\Delta\epsilon_{max} = 0.7\ M^{-1}\ cm^{-1}$ vs 18,260 cm^{-1} for [$Ni^{II}(SOD^{M1})$]), and the high-energy positive signed feature at 28 735 cm^{-1} (($\Delta\epsilon_{max} = 2.4\ M^{-1}\ cm^{-1}$ vs 29 130 cm^{-1} for [$Ni^{II}(SOD^{M1})$]). Thus, the electronic structure of the two metallopeptides are similar to one another, again indicating that the residues outside of the Ni-binding hook are not significantly contributing to the electronic structure of the Ni-center in [$Ni^{II}(SOD^{M1})$].

The electronic absorption and CD spectra of [$Ni^{II}(SOD^{M2}$H-(1)D)] and [$Ni^{II}(SOD^{M2}H(1)A)$] both compare well with that of [$Ni^{II}(SOD^{M2})$] (Figure 4), including the characteristic Ni-($3d_{xy}$)/S(π)* → Ni($3_{x^2-y^2}$/S/N(σ))* transitions at 21 785 cm^{-1} ([$Ni^{II}(SOD^{M2}H(1)A)$]; 459 nm; $\epsilon = 427\ M^{-1}\ cm^{-1}$) and 21 945 cm^{-1} ([$Ni^{II}(SOD^{M2}H(1)D)$]; 456 nm; $\epsilon = 325\ M^{-1}\ cm^{-1}$). This indicates that the electronic structures (and presumably the Ni^{II} coordination environments) of the three metallopeptides are nearly identical (Table 1). This supposition was further supported by Ni K-edge X-ray absorption spectroscopy.

Figure 5 depicts the Ni K-edge X-ray absorption spectrum and refinements to the EXAFS data for [$Ni^{II}(SOD^{M2})$]. The edge region of the XAS spectrum displays a weak 1s → 3d transition at 8332.1(1) eV (area = 0.02(1) eV relative to the edge) and a relatively intense 1s → $4p_z$ transition at 8338.3(1) eV (area [Ni^{II}-(SOD^{M2})] = 0.37(1) eV relative to the edge), which are indicative of square planer Ni^{II}.[43] This is similar to the pre-edge transitions observed in both [$Ni^{II}(SOD^{M2}H(1)A)$] and [Ni^{II}-(SOD^{M2}H(1)D)], which are similar in energy and intensity as those found in [$Ni^{II}(SOD^{M2})$] (Supporting Information). Furthermore, the overall shape of the XANES regions of the XAS are similar for the three metallopeptides, strongly suggesting similar coordination environments.

The EXAFS region of the XAS for [$Ni^{II}(SOD^{M2})$] is best modeled as a four coordinate Ni-center with two Ni−N

(42) Fiedler, A. T.; Bryngelson, P. A.; Maroney, M. J.; Brunold, T. C. *J. Am. Chem. Soc.* **2005**, *127*, 5449−5462.

(43) Colpas, G. J.; Maroney, M. J.; Bagyinka, C.; Kumar, M.; Willis, W. S.; Suib, S. L.; Mascharak, P. K.; Baidya, N. *Inorg. Chem.* **1991**, *30*, 920−928.

Table 1. Physical Properties of [$Ni^{II}(SOD^{M2}H(1)X)$]

		mass (Da)		electronic absorption	CD	$E_{1/2}$[a]
	K_d (μM)	ESI-MS	GPC	λ (cm^{-1}) (ϵ(M^{-1} cm^{-1}))	λ (cm^{-1}) ($\Delta\epsilon$(M^{-1} cm^{-1}))	V (Ag/AgCl)
[$Ni^{II}(SOD^{M2})$]	5(1)	798.5	793	27,625 (sh, 656)[b] 21,900 (345) 18,250 (sh, 130)[b] 12,150 (sh, 50)[b]	28,735 (2.4) 22,220 (−1.5) 17,635 (0.7) 14,190 (−0.4) 11,400 (0.9)	0.52(1)
[$Ni^{II}(SOD^{M2}H(1)A)$]	6(3)	732.1	768	21,785 (427) 18,415 (sh, 252)[b] 12,600 (sh, 50)[b]	24,860 (1.0) 21,030 (−2.2) 17,640 (0.4) 15,470 (0.5) 12,130 (0.4)	0.67(1)
[$Ni^{II}(SOD^{M2}H(1)D)$]	7(2)	755.6	810	28,245 (sh, 418)[b] 21,945 (325) 18,245 (sh, 127)[b] 12,190 (sh, 40)	30,400 (3.4) 25,330 (0.8) 20,920 (−1.2) 16,400 (0.3) 13,890 (−0.2) 11,760 (0.6)	0.48(1)

[a] Reported $E_{1/2}$ values for the Ni^{II}/Ni^{III} couple are from the solution cyclic voltammetry data. [b] sh = shoulder, and the subsequent ϵ at the energy indicated.

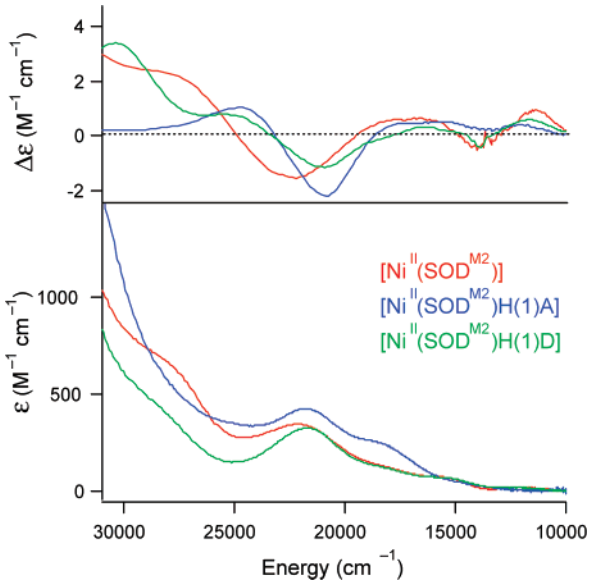

Figure 4. Electronic absorption (bottom) and CD (top) spectra of [$Ni^{II}(SOD^{M2})$] (red), [$Ni^{II}(SOD^{M2}H(1)A)$] (blue), and [$Ni^{II}(SOD^{M2}H(1)D)$] (green). The discontinuity in the CD spectra at 13 350 cm^{-1} (most apparent in the spectrum of [$Ni^{II}(SOD^{M2})$]) is due to a manual detector change at that energy.

Chart 1

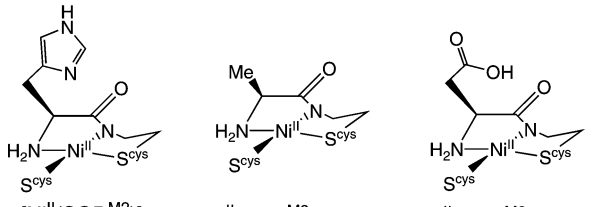

scatterers at 1.875(3) Å and two Ni−S scatterers at 2.176(3) Å (Table 2, Chart 1), which compares well with the EXAFS refinements obtained for [$Ni^{II}(SOD^{M1})$][18] and the crystallographic data of reduced NiSOD.[13,14] Like [$Ni^{II}(SOD^{M2})$] an EXAFS analysis demonstrates that both [$Ni^{II}(SOD^{M2}H(1)A)$] and [$Ni^{II}(SOD^{M2}H(1)D)$] contain Ni^{II} in square planar N_2S_2 coordination environments with similar average Ni−S (~2.17 Å) and Ni−N (~1.88 Å) bond lengths (Table 2, Chart 1, Supporting Information). This further supports the conclusions reached from the optical and CD studies that the Ni^{II} centers of [$Ni^{II}(SOD^{M2})$], [$Ni^{II}(SOD^{M2}H(1)D)$], and [$Ni^{II}(SOD^{M2}H(1)A)$] are all contained in similar coordination environments and are representative of the reduced NiSOD active-site structure.

The cyclic voltammogram (CV) of [$Ni^{II}(SOD^{M2})$] obtained at 25 °C in solution (1.0 mM [$Ni^{II}(SOD^{M2})$], 100 mM $NaClO_4$-(aq), pH 7.4) displays quasireversible behavior for the Ni^{II}/Ni^{III} couple at 0.52(1) V versus Ag/AgCl. The peak-to-peak separation of 240 mV is suggestive of a substantial structural rearrangement taking place at the Ni-center upon oxidation/reduction. This behavior will be explored in detail in the next section. Similar to the electrochemical behavior of [$Ni^{II}(SOD^{M2})$] the CV obtained for [$Ni^{II}(SOD^{M2}H(1)D)$] recorded under identical conditions also displays a quasireversible Ni^{II}/Ni^{III} couple at a slightly more negative potential of 0.48(1) V versus Ag/AgCl. Also similar to [$Ni^{II}(SOD^{M2})$], the large peak to peak separation (260 mV) is indicative of significant structural rearrangement taking place about the Ni-center upon oxidation/reduction. In contrast to the electrochemical behavior of [$Ni^{II}(SOD^{M2})$] and [$Ni^{II}(SOD^{M2}H(1)D)$], the CV obtained for [$Ni^{II}(SOD^{M2}H(1)A)$] displays near reversible behavior (ΔE_p = 105 mV) and a significant positive shift in the $E_{1/2}$ to 0.62 V versus Ag/AgCl. The electrochemical data are displayed in Figure 6 and summarized in Table 1.

The Ni^{III} forms of these metallopetides cannot be isolated in pure form for further analysis following chemical oxidation or bulk electrolysis, as we have observed for our other metallopeptide based NiSOD model systems.[18,19] However, we have been able to trap out [$Ni^{III}(SOD^{M2})$] in an EPR tube following its oxidation by substoichiometric amounts of KO_2 (Figure 7). The 77 K EPR spectrum displays g-values characteristic of square pyramidal N-ligated Ni^{III} (g_x = 2.32; g_y = 2.26; g_z = 2.02; A_{zz} = 25.2 G), and is similar to the EPR spectrum of oxidized NiSOD (g_x = 2.30; g_y = 2.24; g_z = 2.01; A_{zz} = 24.9 G).[16] This indicates that the observed wave in the CVs are Ni^{II}/Ni^{III} couples, and the Ni^{III} coordination environment of [$Ni^{III}(SOD^{M2})$] is similar to oxidized NiSOD (i.e., a five coordinate $Ni^{III}N_3S_2$ coordination environment with axial N-ligation; Figure 1). Additional evidence that these are Ni-centered oxidation couples (as opposed to ligand-centered oxidation couples) comes

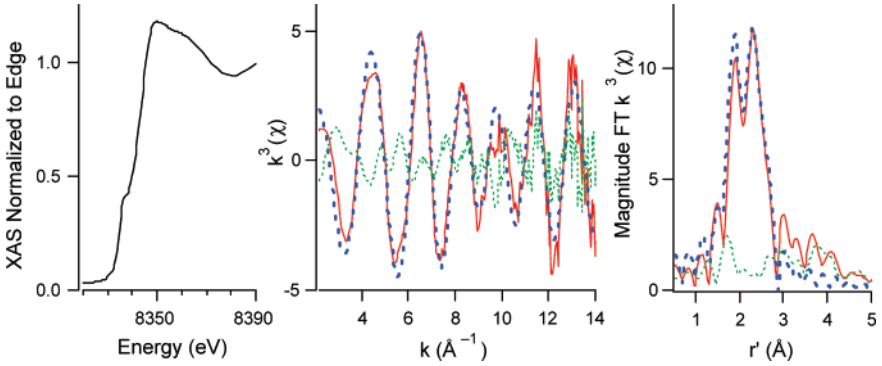

Figure 5. Ni K-edge X-ray absorption spectrum obtained for [$Ni^{II}(SOD^{M2})$]. The left most spectrum displays the XANES region of the XAS, the middle spectrum displays the k^3 EXAFS data, and the right most spectrum displays the magnitude FT k^3 EXAFS. The EXAFS data are presented as the red solid lines, the simulations to the EXAFS data are presented as the blue broken lines, and the green dotted lines display the difference between the experimental and simulated spectra.

Table 2. Best Fits to the EXAFS Data Obtained for [$Ni^{II}(SOD^{M2}H(1)X)$]

	[$Ni^{II}(SOD^{M2})$]	[$Ni^{II}(SOD^{M2}H(1)A)$]	[$Ni^{II}(SOD^{M2}H(1)D)$]
E_o (eV)[a]	8343.3	8342.7	8342.0
n_N[b]	2	2	2
r_N (Å)	1.875(3)	1.898(6)	1.874(8)
σ_N^2 (Å^2)	0.0028(3)	0.0024(10)	0.0024(7)
n_S[b]	2	2	2
r_S (Å)	2.176(3)	2.166(1)	2.168(4)
σ_S^2 (Å^2)	0.0036(1)	0.0028(2)	0.0037(2)
ϵ^2	0.86	0.87	0.61

[a] For all four refinements E_o was initially refined for the S-shell and then restrained to this value for all shells in subsequent refinement cycles. [b] The number of scatters was initially a refinable parameter and then restrained to the nearest whole number in the final refinements.

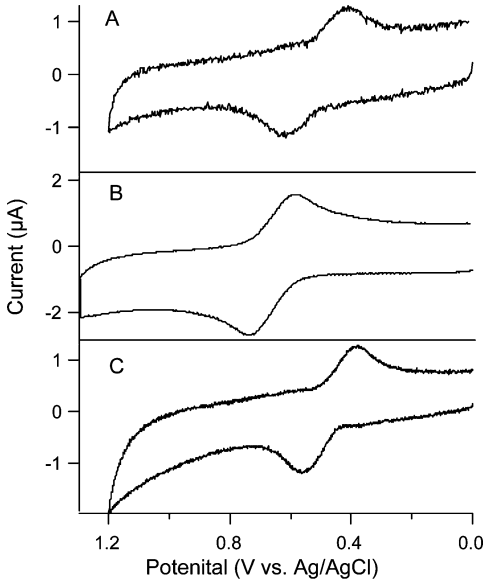

Figure 6. Cyclic voltammograms obtained for 1.0 mM solutions of [Ni(SOD^{M2})] (A), [Ni($SOD^{M2}H(1)A$)] (B), and [Ni($SOD^{M2}H(1)D$)] (C) at pH 7.4 (100 mM $NaClO_4$ (aq)) and a scan velocity of 100 mV s^{-1}.

from the fact that (1) there are no side chains in our peptide sequence that would give a reversible one-electron couple in this region and (2) $Ni^{II}N_2S_2$ complexes that undergo ligand-centered (at the ligated sulfurs) one-electron oxidations display completely irreversible oxidation couples.[20,44]

(44) (a) Grapperhaus, C. A.; Mullins, C. S.; Kozlowski, P. M.; Mashuta, M. S. *Inorg. Chem.* **2004**, *43*, 2859−2866. (b) Grapperhaus, C. A.; Darensbourg, M. Y. *Acc. Chem. Res.* **1998**, *31*, 451−459.

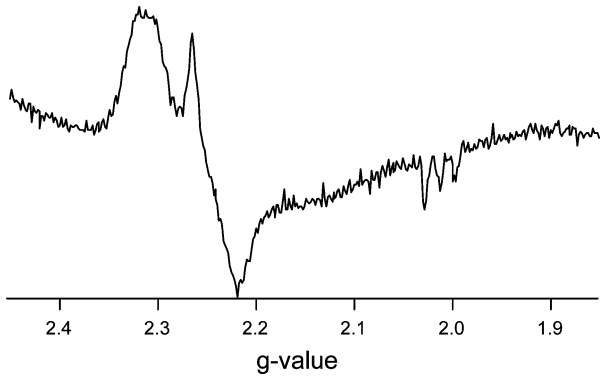

Figure 7. EPR spectrum of [$Ni^{III}(SOD^{M2})$] recorded at 77 K.

From these electrochemical data a number of conclusions can be drawn. First, these data strongly indicate that the axial ligand provided by the N-terminal residue is coming on and off upon oxidation/reduction *at these relatively slow scan velocities*. Both [Ni(SOD^{M2})] and [Ni($SOD^{M2}H(1)D$)] display large peak separations while [Ni($SOD^{M2}H(1)A$)], which possesses an N-terminal residue that lacks a potential axial ligand to Ni^{III}, displays a considerably smaller peak-to-peak separation. These data also suggest that the axial ligand significantly stabilizes the Ni^{III} oxidation state, as has previously been demonstrated.[45] Both [Ni(SOD^{M2})] and [Ni($SOD^{M2}H(1)D$)] display an oxidation peak ∼250 mV more negative in potential than [Ni($SOD^{M2}H(1)A$)], demonstrating the stabilization of the Ni^{III} oxidation state in [$Ni^{III}(SOD^{M2})$] and [$Ni^{III}(SOD^{M2}H(1)D)$] relative to [Ni($SOD^{M2}H(1)A$)]. Last, these data suggest that [Ni(SOD^{M2})], [Ni($SOD^{M2}H(1)D$)], and [Ni($SOD^{M2}H(1)A$)] should all be capable of behaving as SODs. The redox potential for these metallopeptides all fall in between the $O_2^{\bullet-}$ oxidation and reduction couples of −0.04 and 1.09 V versus Ag/AgCl. We probed this supposition by performing SOD activity assays on these three metallopeptides.

SOD Activities of [Ni(SOD^{M2})], [Ni($SOD^{M2}H(1)A$)], and [Ni($SOD^{M2}H(1)D$)]. Metallopeptide SOD activities were measured using a modified xanthine/xanthine oxidase assay.[23] In this assay a steady-state concentration of $O_2^{\bullet-}$ is produced in solution from the reaction of xanthine oxidase with xanthine. The $O_2^{\bullet-}$ in turn reduces nitro blue tetrazolium (NBT, a colorless compound) into formazan, a highly colored blue compound

(45) Krüger, H.-J.; Peng, G.; Hom, R. H. *Inorg. Chem.* **1991**, *30*, 734−742.

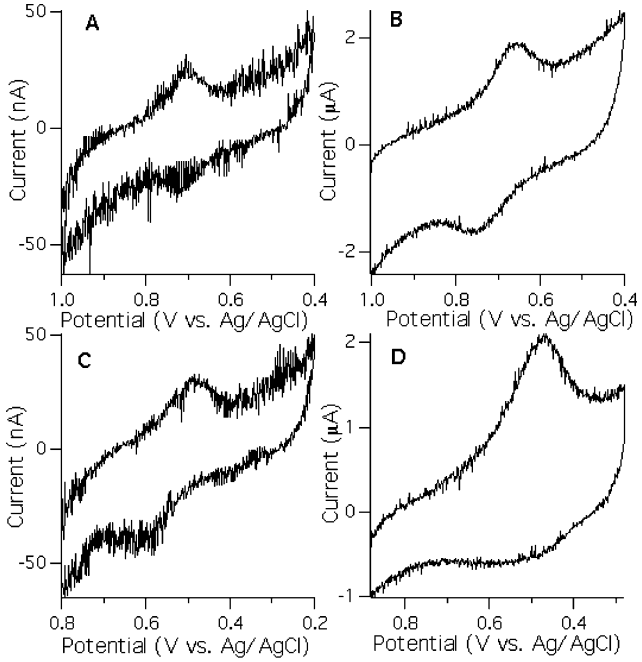

Figure 8. The top left and right cyclic voltammograms are of [Ni(SOD^{M2}H-(1)A)] immobilized in DDAB bilayers recorded at scan rates of 10 mV s^{-1} (A) and 50 V s^{-1} (B). The bottom left and right cyclic voltammograms are of [Ni(SOD^{M2})] immobilized in DDAB bilayers recorded at scan rates of 10 mV s^{-1} (C) and 10 V s^{-1} (D).

($\epsilon_{560\ nm} \approx 35{,}000\ M^{-1}\ cm^{-1}$).[46] The concentration of a SOD active compound required to effect a 50% reduction in the rate of formazan production is referred to as the IC_{50} concentration. [Ni^{II}(SOD^{M2})] displays an IC_{50} of $1(1) \times 10^{-6}$ M, which is comparable to synthetic SODs reported in the literature.[47] For comparison to a naturally occurring SOD, Cu/ZnSOD yields an IC_{50} of 4×10^{-8} M by this assay, suggesting that [Ni^{II}-(SOD^{M2})] affords an SOD disproportion rate ~25 fold slower than the natural system (k_{cat} for Cu/Zn SOD is $\approx 2 \times 10^9\ M^{-1}\ s^{-1}$), and is thus a competent SOD.[23,48]

Both [Ni^{II}(SOD^{M2}H(1)D)] and [Ni^{II}(SOD^{M2}H(1)A)] display reduced SOD activities in comparison to [Ni^{II}(SOD^{M2})]. [Ni^{II}-(SOD^{M2}H(1)D)] displays an IC_{50} of $5(2) \times 10^{-6}$ M, which although lower than [Ni^{II}(SOD^{M2})], is still comparable. [Ni^{II}-(SOD^{M2}H(1)A)] displays substantially reduced SOD activity with an $IC_{50} = 3(2) \times 10^{-5}$ M, over an order of magnitude poorer than the parent [Ni^{II}(SOD^{M2})]. We note that solutions of either $NiCl_2$ or the apo-peptides do not affect a 50% reduction in the rate of formazan production at concentrations exceeding 1×10^{-4} M, demonstrating that trace amounts of unligated Ni^{II} or peptide are not contributing significantly to $O_2^{\bullet-}$ degradation.

By following the production of uric acid, we determined that after 1 min the concentration of $O_2^{\bullet-}$ produced by this xanthine/xanthine oxidase assay was 11(1) μM. This leads to the possibility that [Ni^{II}(SOD^{M2}H(1)A)] is not catalytic, and we are only observing the oxidative half-reaction (Ni^{II} → Ni^{III}). We therefore performed a second NBT competition assay. Here a solution of 30 μM NBT was combined with 10 μM [Ni^{II}-(SOD^{M1}H(1)X)] in 50 mM NEM buffer (pH = 7.4) and KO_2 was added. If the metallopeptides are not present in solution the addition of 50 equiv of KO_2 effected the complete conversion of NBT into formazan (see Supporting Information). In contrast, it is not until over 4000 equiv of KO_2 was added to solutions of NBT/[Ni^{II}(SOD^{M1})] or NBT/[Ni^{II}(SOD^{M1}H(1)D)] that we observed the complete conversion of NBT to formazan. [Ni^{II}(SOD^{M1}H(1)A)] was significantly less active, with only 1500 equiv of KO_2 required to observe the complete conversion of NBT into formazan. In control experiments $NiCl_2$ and the apo-peptides themselves provid no protection to NBT against reduction to formazan by $O_2^{\bullet-}$. Because a large excess of KO_2 relative to the metallopeptides needs to be added to solution to affect the complete conversion of NBT to formazan it appears that all three of these metallopeptides will catalytically disproportionate $O_2^{\bullet-}$.

Altogether, these data suggest two important findings. One is that an axial ligand provided to Ni in general appears to optimize the NiSOD active site for catalysis. The second important finding is that lack of an axial ligand does not completely cut off the metallopeptide's SOD activity, just diminishes it.

Metallopeptide Thin-Film Voltammetry. To obtain information concerning the kinetics of the electron transfer (ET) taking place during the Ni^{II}/Ni^{III} redox process in [Ni^{II}(SOD^{M2})] versus [Ni^{II}(SOD^{M2}H(1)A)] we utilized fast-scan thin-film voltammetry. By immobilizing the metallopeptides as thin films on a pyrolytic graphite electrode surface diffusion of the metallopeptides away from the electrode no longer complicates the electrochemical studies. Therefore fast scan rates can be used to probe the presence of transient electroactive species. For these studies we immobilized either [Ni^{II}(SOD^{M2})] or [Ni^{II}-(SOD^{M2}H(1)A)] in a dimethyldidodecylammonium bromide (DDAB) surfactant bilayer according to the methods of Rusling et al.[28] This method of immobilizing the metallopeptides yielded excellent and reproducible electrochemical responses over scan velocities ranging from 0.005 to 50 V s^{-1} (Figure 8). Other procedures for immobilizing the metallopeptides on the electrode surface,[32,49] such as using neomycin or polymyxin B sulfate as coadsorbants, gave poor results.

For [Ni^{II}(SOD^{M2}H(1)A)] as the scan rate is increased from 5 mV s^{-1} to 50 V s^{-1} one observes an increase in the peak to peak separation. Although the peaks display mostly Nernstian behavior throughout the window of scan rates used, we do observe a slight broadening and asymmetry of the oxidative and reductive peaks at fast scan rates (Figure 9). The variation in peak separation as a function of scan rate obeys an exponential relationship. At slow scan rates (less than 1 V s^{-1}) the peak to peak separations are on the order of ~30 mV, but as the scan rate increases beyond 10 V s^{-1} the peaks sharply begin to separate. A plot of the peak separation versus the log of the scan rate yields a well behaved "trumpet" plot (Figure 9),[31,50,51] which is indicative of reversible electrochemical

(46) Bielski, H. J.; Shiuw, G. G.; Bajuk, S. J. *J. Phys. Chem.* **1980**, *84*, 830.
(47) For example see: (a) Ohtsu, H.; Shimazaki, Y.; Odani, A.; Yamauchi, O.; Mori, W.; Itoh, S.; Fukuzumi, S. *J. Am. Chem. Soc.* **2000**, *122*, 5733. (b) Li, D.; Li, S.; Yang, D.; Yu, J. Huang, J.; Li, Y.; Tang, W. *Inorg. Chem.* **2003**, *42*, 6071−6080. (c) Kitajima, N.; Osawa, M.; Tamura, N.; Morooka, Y.; Hirano, T.; Hirobe, M.; Nagano, T. *Inorg. Chem.* **1993**, *32*, 1879−1880. (d) Devereux, M.; O'Shea, D.; Kellett, A.; McCann, M.; Walsh, M.; Egan, D.; Deegan, C.; Kedziora, K.; Rosair, G.; Mueller-Bunz, H. *J. Inorg. Biochem.* **2007**, *101*, 881−892.
(48) Pierre, J.-L.; Chautemps, P.; Refaif, S.; Beguin, C.; El, Mazouki, A.; Serratrice, G.; Saint-Aman, E.; Rey, P. *J. Am. Chem. Soc.* **1995**, *117*, 1965.
(49) Boll, M.; Fuchs, G.; Tilley, G.; Armstrong, F. A.; Lowe, D. J. *Biochemistry* **2000**, *39*, 4929−4938.
(50) Vincent, K. A.; Armstrong, F. A. *Inorg. Chem.* **2005**, *44*, 798−809.
(51) Elliott, S. J.; Hoke, K. R.; Heffron, K.; Palak, M.; Rothery, R. A.; Weiner, J. H.; Armstrong, F. A. *Biochemistry*, **2004**, *43*, 799−807.

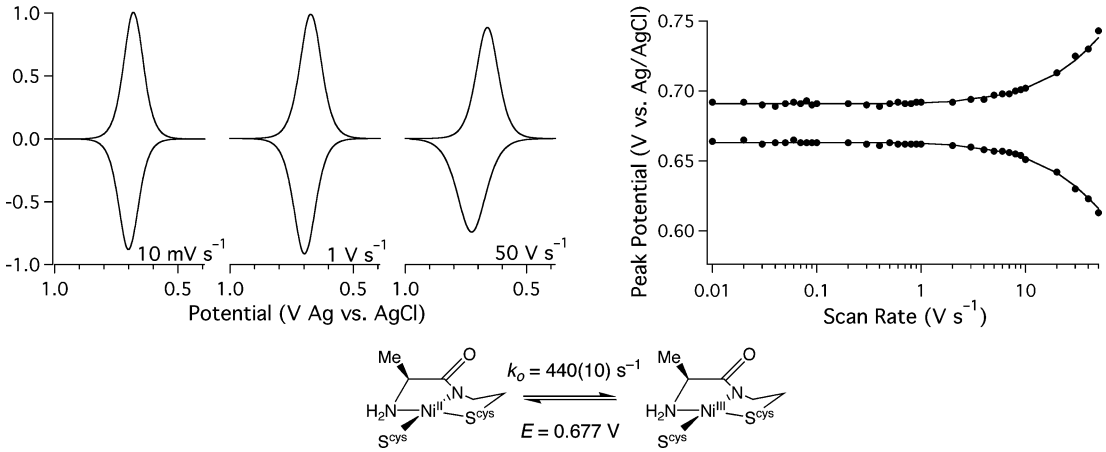

Figure 9. The left-hand graphs depict the electrochemical data obtained for [Ni^{II}(SOD^{M2}H(1)A)] recorded over a variety of scan rates. The data is presented with the background capacitance removed and the voltammograms normalized. The plot to the right depicts the peak position in the voltammograms as a function of scan rate (closed circles) and simulations to the data (lines) using a $k_o = 440$ s−1 and an $E = 0.667$ V vs Ag/AgCl (as outlined in the Scheme at the bottom). The simulation also includes a peak separation of 24 mV.

behavior. These data were modeled using standard Butler−Volmer kinetics:

$$k_{red} = k_o \exp[-\alpha nf(E_{app} - E)] \quad (11)$$

$$k_{ox} = k_o \exp[(1 - \alpha)nf(E_{app} - E)] \quad (12)$$

where k_o is the standard rate constant at zero overpotential, α is the transfer coefficient (set to 0.5), $f = (F/RT)$, E_{app} is the applied electrochemical potential, and E is the potential of the Ni^{II}/Ni^{III} redox process.[52] The data were best modeled as a simple one-electron redox process (Figure 8) with a $k_o = 440$-(10) s^{-1} and an $E = 0.677(5)$ V versus Ag/AgCl. The value of k_o is consistent with facile ET to and from the Ni-center in [Ni^{II}-(SOD^{M2}H(1)A)], and is comparable with the k_o obtained for proteins such as the *Sulfolobus acidocaldarius* ferredoxin[31] and P450 Fe-heme centers.[54]

In contrast to the relatively straight forward ET kinetics displayed by [Ni^{II}(SOD^{M2}H(1)A)], the electrochemical data for [Ni^{II}(SOD^{M2})] displays far more complex behavior as a function of scan rate (Figure 10). From an oxidative poise at low scan velocities (<500 mV) there is a relatively large peak to peak separation of ∼120 mV. At intermediate scan velocities the reoxidation wave disappears into the baseline and then reappears at faster scan rates (>10 V s^{-1}), with much closer peak to peak separations than observed at slow scan rates (∼30 mV). Furthermore at these faster scan rates the oxidation wave is significantly broadened. This behavior has been noted by others and is suggestive that the reoxidation step is preceded by a "gating" process.[32,54,55] For [Ni(SOD^{M2})] reduction of the Ni-(III) center involves deligation of the imidazole ligand to Ni at slow scan rates, and reoxidation of four coordinate Ni(II) to four-coordinate Ni(III) is observed. At fast scan rates the imidazole remains ligated throughout the redox process, and the reoxidation of five-coordinate Ni(II) to five-coordinate Ni-(III) is observed as a broad wave. In the intermediate scan-rate regime both processes are occurring, resulting in a broad oxidation wave that is blurred into the background. From a reductive poise a plot of peak position versus scan rate yields an identical plot for the reduction waves. The only difference observed is that the oxidation waves yields a straight line for the plot of peak position versus scan rate that is centered about 0.63 V versus Ag/AgCl, which is invariant with scan velocity.

The electrochemical data for [Ni(SOD^{M2})] were modeled using a square kinetic scheme (Figure 10).[49,54] The rate constants calculated for ET to and from [Ni(SOD^{M2})] are nearly identical to the $k_o = 440(10)$ s^{-1} obtained for [Ni(SOD^{M2}H(1)A)]. We find that the redox process for conversion between four-coordinate Ni^{II}/Ni^{III} and five-coordinate Ni^{II}/Ni^{III} each occurs with similar standard rate constants (with $k_o = 440(20)$ s^{-1} (four-coordinate Ni) and $k_o' = 450(20)$ s^{-1} (five-coordinate Ni)). The main difference between the two redox processes is the large negative shift in the redox potential upon going from four- to five-coordinate Ni. The four-coordinate Ni^{II}/Ni^{III} couple occurs at 0.593(10) V versus Ag/AgCl (versus $E = 0.677(5)$ V versus Ag/AgCl for four-coordinate [Ni(SOD^{M2}H(1)A)]). In contrast, the Ni^{II}/Ni^{III} couple for five-coordinate [Ni(SOD^{M2})] occurs at 0.452(15) V versus Ag/AgCl, which is consistent with the findings that a five coordinate geometry aids in stabilizing the Ni^{III} oxidation state in Ni-thiolate complexes relative to a four-coordinate square-planar geometry.

These data indicate that upon accessing the Ni^{III} oxidation state the imidazole from H(1) of [Ni(SOD^{M2})] rapidly coordinates to the Ni-center ($k_{on} = 615(50)$ s^{-1}), with five-coordinate [Ni^{III}(SOD^{M2})] strongly favored over the four-coordinate form of the oxidized metallopeptide ($K_{on} = 3075(200)$). Reduction of [Ni^{III}(SOD^{M2})] results in the slow loss of the axial imidazole ligand ($k_{off} = 7(5)$ s^{-1}), with four-coordinate [Ni^{II}(SOD^{M2})] slightly more favored over five-coordinate [Ni^{II}(SOD^{M2})] ($K_{off} = 12(10)$ s^{-1}).

Altogether these data yield several insights concerning NiSOD. One is that ET to and from the four- and five-coordinate Ni^{II}/Ni^{III} centers are rapid. This demonstrates that these Ni-centers are in fact set up for fast ET as implied by the rapid k_{cat}

(52) Bard, A. J.; Faulkner, L. R.; *Electrochemical Methods: Fundamentals and Applications*, 2nd ed.; John Wiley & Sons: New York, NY, 2001.
(53) (a) Udit, A. K.; Hindoyan, N.; Hill, M. G.; Arnold, F. H.; Gray, H. B. *Inorg. Chem.* **2005**, *44*, 4109−4111. (b) Udit, A. K.; Hill, M. G.; Bittner, V. G.; Arnold, F. H.; Gray, H. B. *J. Am. Chem. Soc.* **2004**, *33*, 10218−10219.
(54) Jeuken, L. J. C.; van Vliet, P.; Verbeet, M. Ph.; Camba, R.; McEvoy, J. P.; Armstrong, F. A.; Canters, G. W. *J. Am. Chem. Soc.* **2000**, *122*, 12186−12194.
(55) (a) Hoffman, B. M.; Ratner, M. R. *J. Am. Chem. Soc.* **1987**, *109*, 6237−6243. (b) Bond, A. M.; Oldham, K. B. *J. Phys. Chem.* **1983**, *87*, 2492−2502.

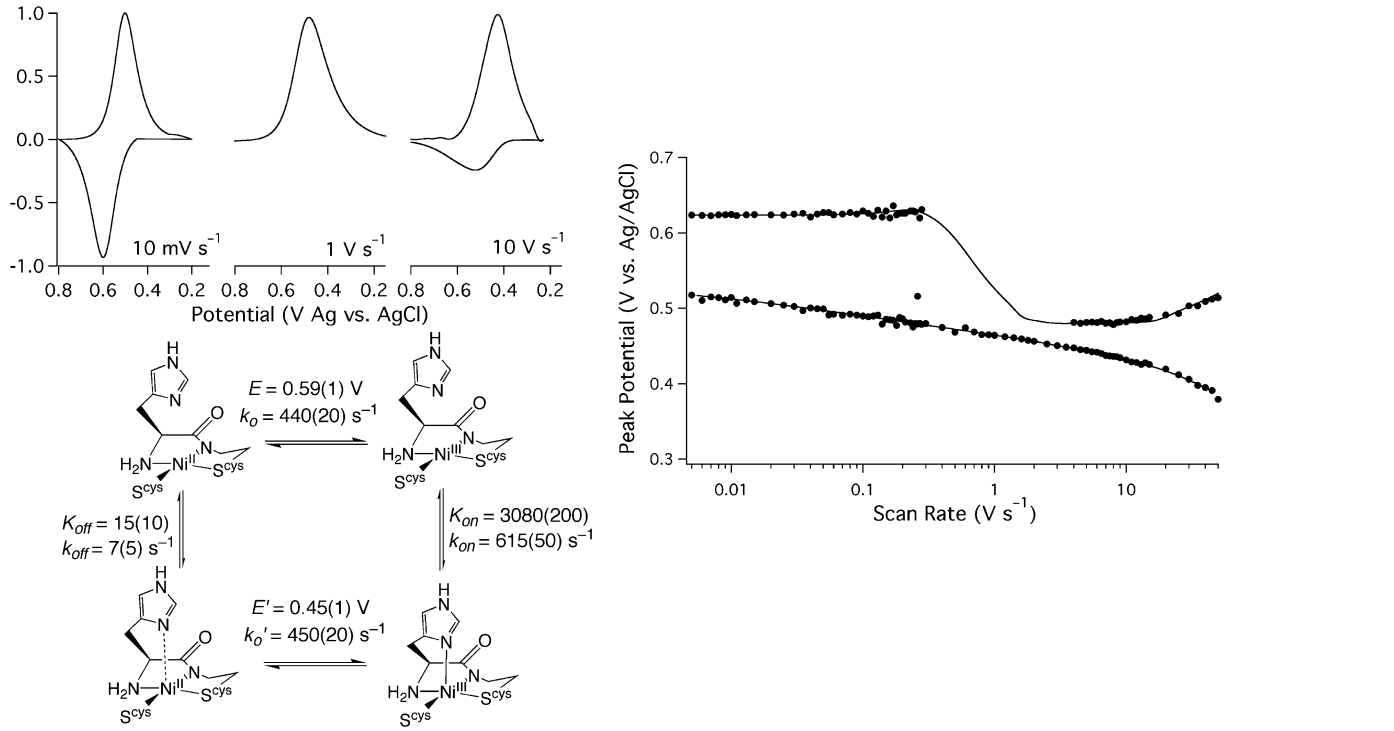

Figure 10. The left-hand graphs depict the electrochemical data obtained for [$Ni^{II}(SOD^{M2})$] recorded over a variety of scan rates. The data is presented with the background capacitance removed and the voltammograms normalized. The plot to the right depicts the peak position in the voltammograms as a function of scan rate (closed circles) and simulations to the data (lines). Over the scan velocities ranging from 0.215 to 3.200 V s^{-1} the data were less than 10% of that recorded at 5 mV s^{-1}, and therefore peak positions could not be reliably extracted from the voltammetry data. The simulation parameters are outlined in the square scheme depicted at the bottom left.

value obtained for NiSOD ($k_{cat} > 2 \times 10^9$ M^{-1} s^{-1}).[15,16] Also, these data suggest that the axial imidazole likely remains ligated to the Ni-center throughout SOD catalysis in the case of [Ni-(SOD^{M2})], and by analogy NiSOD. This supposition comes from the fact that the equilibrium and rate constants for imidazole ligation/dissociation show a strong preference for five- versus four-coordinate Ni^{III} and only a slight preference for four- versus five-coordinate Ni^{II}; k_{off} and K_{off} for [$Ni^{II}(SOD^{M2})$] are 2 orders of magnitude smaller than the values of k_{on} and K_{on}. Also, we note that the first-order rate of $O_2^{\bullet-}$ disproportionation observed in the xanthine/xanthine oxidase assay (~80 s^{-1})[56] is faster than the rate of imidazole deligation by approximately an order of magnitude, while the rate of imidazole binding is faster than superoxide disproportionation by approximately an order of magnitude.

We therefore propose the mechanism outlined in Scheme 1 for the disproportionation of $O_2^{\bullet-}$ by NiSOD, which involves oxidation of the four-coordinate Ni^{II} center followed by rapid imidazole coordination. Once the imidazole is coordinated to the oxidized Ni^{III} center it will remain ligated throughout catalysis. Although Scheme 1 depicts the coordinated imidazole remaining protonated while ligated to Ni^{III}/Ni^{II}, it should be noted that we have no evidence for or against this. Therefore the coordinated imidazole may very well be deprotonated while ligated to the Ni-center.

Reorganization Energy Probed by DFT and ET Rates at Overpotential. The above electrochemical data demonstrate that the Ni-centers of both [Ni(SOD^{M2})] and [Ni(SOD^{M2}H(1)A)] are capable of undergoing fast ET processes between the Ni^{II} and

Scheme 1

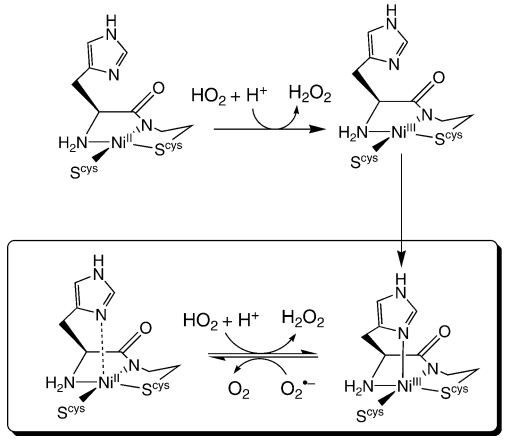

Ni^{III} states. However, the observed rate constants are for ET at zero overpotential. To determine what the ET rate constants would be at the potentials required for $O_2^{\bullet-}$ oxidation/reduction the reorganization energy (λ) must be determined.[57] Since the Ni^{III} states of these metallopeptides cannot be isolated for detailed analysis we turned our attention to electronic structure calculations to estimate the inner-sphere reorganization energy (λ_i) for these metallopeptides.

Minimized metallopeptides based on the crystal structures of reduced and oxidized NiSOD were constructed as follows. The Cartesian coordinates for the heavy atoms of H(1), C(2), C(6), and Ni were placed according to their positions from the crystallographic data of reduced and oxidized NiSOD followed by an idealized placement of the hydrogen atoms.[13,14] The C=

(56) This is estimated from the IC_{50} concentration of Cu/Zn SOD coupled with its second order rate of $O_2^{\bullet-}$ disproportionation.

(57) Marcus, R. A. *Rev. Mod. Phys.* **1993**, *65* 599−610.

Chart 2

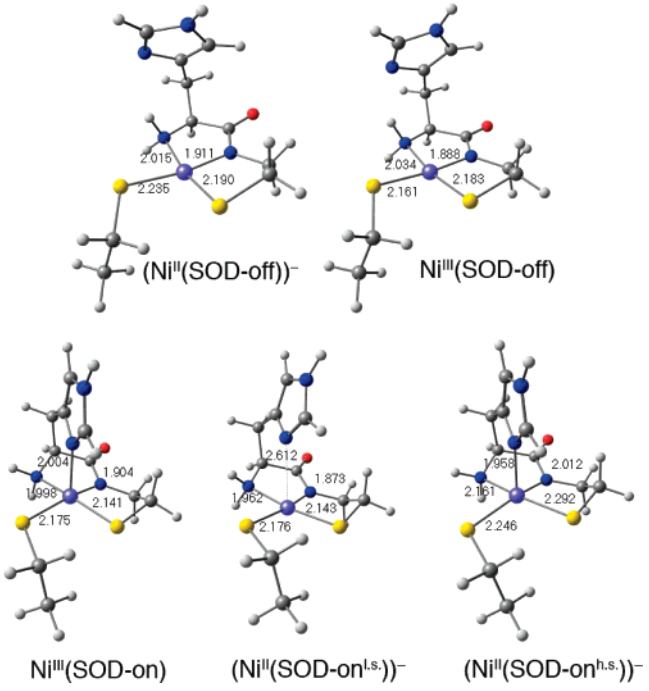

O group from C(2) was removed and C(6) was trimmed down to the corresponding ethanethiolate. Energy minimizations of the oxidized (Ni^{III}(SOD-on)) and reduced ((Ni^{II}(SOD-off))$^-$) NiSOD computational models were performed by DFT methods (Chart 2). For simplicity in calculating λ_i we chose to explore only those models that have the imidazole protonated throughout ET.

The resulting structures of Ni^{III}(SOD-on) and (Ni^{II}(SOD-off))$^-$ compare well with the crystal structure of NiSOD,[13,14] related synthetic NiN_2S_2 complexes,[20] and previous computational studies.[20,42,44a,58] For (Ni^{II}(SOD-off))$^-$ the model minimizes to a structure with Ni−N distances of 2.015 (amine) and 1.911 Å (amide), while the Ni−S distances are 2.235 (trans to the amide N) and 2.190 Å (trans to the amine). When compared to reduced NiSOD[14] and the related $Ni^{II}N_2S_2$ complex (Ni^{II}(BEAAM))$^-$,[20] both the Ni−N and Ni−S distances are overestimated by less than 0.1 Å, which should have a minimal impact on the resulting DFT energies when compared to better optimized computational models.[59] Similarly the equatorial Ni−N (Ni−N^{amine}, 1.998 Å; Ni−N^{amide}, 1.904 Å) and Ni−S bond lengths (Ni−S trans amide, 2.175 Å; Ni−S trans amine, 2.141 Å) of Ni^{III}(SOD-on) are also overestimated by less than 0.1 Å when compared to oxidized NiSOD.[15] We note that in Ni^{III}(SOD-on) the axial N−Ni^{III} bond (derived from the H(1) imidazole) is considerably shorter than that observed in the crystal structure of oxidized NiSOD (2.004 Å vs ∼2.30 Å). Brunold and co-workers have suggested that the relatively long Ni^{III}-imidazole bond in oxidized NiSOD results from hydrogen bonding between the side-chain of Q(17) and the imidazole from H(1).[42] Considering that such an interaction is not possible in [Ni(SOD^{M2})] no attempt was made to compensate for the "short" Ni^{III} bond length observed in these studies. These bond lengths are summarized in Chart 2.

Utilizing the methods of Jakobson et al.[40] λ_i was calculated for the Ni^{III}(SOD-on)/(Ni^{II}(SOD-off))$^-$ ET self-exchange reaction (eq 5). In this procedure the projected force constants for the atomic displacement of all of the atoms in (Ni^{II}(SOD-off))$^-$ moving to their corresponding positions in Ni^{III}(SOD-on) (and the atoms in Ni^{III}(SOD-on) moving to their corresponding positions in (Ni^{II}(SOD-off))$^-$) are calculated according to eq 9. These projected force constants are then combined as outlined in eq 10 resulting in λ_i. The resulting value for λ_i of 34.8 kcal mol^{-1} is significantly larger than what would be predicted for a system undergoing facile ET. This value is nearly double that observed for several cytochromes,[53b,60a] and at least triple that observed for blue copper centers.[31,60b] This lends further support to the conclusions reached from the electrochemical data that ET precedes imidazole ligation/dissociation and is not concurrent with imidazole ligation/dissociation.

To obtain values for λ_i for the self-exchange reactions where the imidazole remains on or off during ET, force constants and atomic coordinates for imidazole ligated (Ni^{II}(SOD-on))$^-$ and imidazole unligated Ni^{III}(SOD-off) were obtained. This was done by using (Ni^{II}(SOD-off))$^-$ and Ni^{III}(SOD-on) as starting structures, followed by oxidation or reduction of the Ni-center and subsequent geometry optimizations. We were thus able to obtain minimized structures for Ni^{III}(SOD-off), low-spin (Ni^{II}(SOD-on$^{l.s.}$))$^-$, and high spin (Ni^{II}(SOD-on$^{l.s.}$))$^-$ (Chart 2). The computational model obtained for Ni^{III}(SOD-off) possesses Ni−N bond lengths of 2.034 (Ni-amine) and 1.888 Å (Ni-amide) while the Ni−S bond lengths were calculated to be at 2.183 (trans to the amide) and 2.161 Å (trans to the amine). The calculated Ni−N^{amide} and Ni−S bond lengths in this model are thus less than 0.07 Å longer than those reported in the bis-amide $Ni^{III}N_2S_2$ complex Ni^{III}(phmi).[61]

The model obtained for (Ni^{II}(SOD-on$^{l.s.}$))$^-$ possesses Ni−N and Ni−S bond lengths (within the equatorial plane) similar to Ni^{III}(SOD-on) (Ni−N^{amine}, 1.962 Å; Ni−N^{amide}, 1.873 Å; Ni−S^{trans_amide}, 2.176 Å; Ni−S^{trans_amine}, 2.143 Å), while the Ni−N^{imidazole} bond lengthened to 2.612 Å. For (Ni^{II}(SOD-on$^{h.s.}$))$^-$ there was an overall elongation of the equatorial Ni−N and N−S bonds relative to to Ni^{III}(SOD-on) (Ni−N^{amine}, 2.161 Å; Ni−N^{amide}, 2.012 Å; Ni−S^{trans_amide}, 2.246 Å; Ni−S^{trans_amine}, 2.292 Å), while the Ni−N^{imidazole} bond contacts to 1.958 Å. The changes in bond lengths of (Ni^{II}(SOD-on$^{l.s.}$))$^-$/Ni^{III}(SOD-on) versus (Ni^{II}(SOD-on$^{h.s.}$))$^-$ are consistent with the difference in electronic structures of the three species. Upon going from square pyramidal low- to high-spin Ni^{II} an electron from the Ni($3d_{z^2}$)* orbital gets promoted to the Ni($3d_{x^2-y^2}$)* orbital, which leads to an overall elongation of the Ni-ligand bonds in the *xy* plane. This elongation is also be seen upon going from oxidized Ni^{III}(SOD-on) to reduced (Ni^{II}(SOD-on$^{h.s.}$))$^-$, where an electron would be added to the Ni($3d_{x^2-y^2}$)* orbital. Furthermore, a contraction of the Ni-ligand bond along the *z*-axis of (Ni^{II}(SOD-on$^{h.s.}$))$^-$ relative to (Ni^{II}(SOD-on$^{l.s.}$))$^-$ is also observed because of the removal of an electron from the Ni($3d_{z^2}$)* orbital. In contrast the Ni−N bond along the *z*-axis of (Ni^{II}(SOD-on$^{h.s.}$))$^-$ is similar to Ni^{III}(SOD-on) because of the fact each species has singularly occupied Ni($3d_{z^2}$)* orbitals.

(58) Mullins, C. S.; Grapperhaus, C. A.; Kozlowski, P. M. *J. Biol. Inorg. Chem.* **2006**, *11*, 617−625.
(59) Siegbahn, P. E. M. *J. Comput. Chem.* **2001**, *22*, 1634−1645.
(60) (a) Davidson, V. L. *Acc. Chem. Res.* **2000**, *33*, 87−93. (b) Di Bilio, A. J.; Hill, M. G.; Bonander, N.; Karlsson, B. G.; Villahermosa, R. M.; Malmstrom, B. G.; Winkler, J. R.; Gray, H. B. *J. Am. Chem. Soc.* **1997**, *119*, 9921−9922.
(61) Hanss, J.; Krüger, H.-J. *Angew. Chem., Int. Ed.* **1998**, *37*, 360−363.

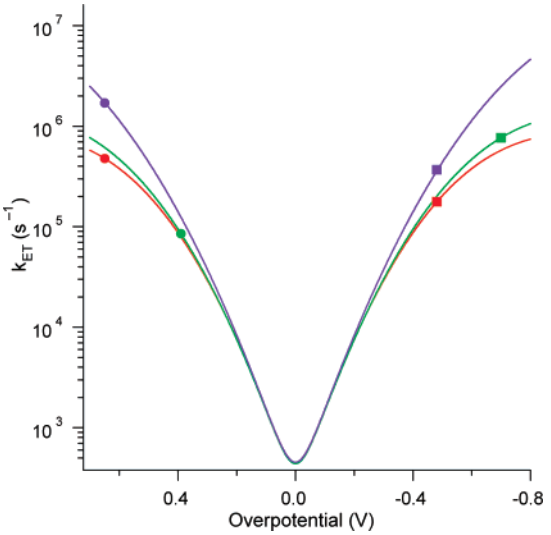

Figure 11. Plot of k_{ET} versus overpotential based on the calculated values for λ_{ET} and experimental values for k_o. The green plot is for the Ni^{III}(SOD-off)/(Ni^{II}(SOD-off))$^-$ ET self-exchange reaction, the red plot is for the Ni^{III}(SOD-on)/(Ni^{II}(SOD-on$^{l.s.}$))$^-$ ET self-exchange reaction, and the purple plot is for the Ni^{III}(SOD-on)/(Ni^{II}(SOD-on$^{h.s.}$))$^-$ ET self-exchange reaction. The values $k_o = 440\ s^{-1}$ and $\lambda_{ET} = 8.1$ kcal mole^{-1} are used for the Ni^{III}(SOD-off)/(Ni^{II}(SOD-off))$^-$ ET reaction, $k_o = 450\ s^{-1}$ and $\lambda_{ET} = 8.0$ kcal mole^{-1} are used for the Ni^{III}(SOD-on)/(Ni^{II}(SOD-on$^{l.s.}$))$^-$ ET reaction, and $k_o = 450\ s^{-1}$ and $\lambda_{ET} = 10.9$ kcal mole^{-1} are used for the Ni^{III}(SOD-on)/(Ni^{II}(SOD-on$^{h.s.}$))$^-$ ET reaction. The overpotentials at which $O_2^{\bullet-}$ oxidation (squares) and reduction (circles) would occur are highlighted.

Using the procedure outline above λ_i for the Ni^{III}(SOD-off)/(Ni^{II}(SOD-off))$^-$ self-exchange ET reaction, (eq 6) was calculated to be 16.2 kcal mole^{-1}, which is comparable to the reorganization energy estimated for some heme centers.[53b,60a] This value of λ_i is therefore reasonable for an ET center. For the Ni^{III}(SOD-on)/(Ni^{II}(SOD-on$^{l.s.}$))$^-$ self-exchange reaction (eq 7) a slightly smaller value of $\lambda_i = 15.9$ kcal mol^{-1} was determined. This indicates that movement of the axial H(1) imidazole along the *z*-axis in this system is facile, with the nearly 0.5 Å elongation of the Ni−N bond upon Ni-center reduction imposing virtually no barrier on the ET reaction. Surprisingly the Ni^{III}(SOD-on)/(Ni^{II}(SOD-on$^{h.s.}$))$^-$ self-exchange reaction (eq 8) yields a relatively large λ_i (21.7 kcal mole^{-1}). The large calculated λ_i results exclusively from the elongation of the two nitrogen- and two sulfur-based ligands along the equatorial plane upon reduction of the Ni^{III} center. We should note that as all of these values are inner-sphere reorganization energies they neglect contributions from the solvent and the rest of the peptide scaffold not included in the computational model.

Using the calculated values for λ_i and the experimentally derived values for k_o ET rate constants (k_{ET}) as a function of overpotential were were obtained. As these λ_i values are for self-exchange reactions the value for λ used in the ET calculations (λ_{ET}) are half those calculated above. These are summarized in Figure 10. Since we have no evidence if (Ni^{II}(SOD-on$^{h.s.}$))$^-$ or (Ni^{II}(SOD-on$^{l.s.}$))$^-$ is the Ni^{II} species present in the Ni^{III}(SOD-on)/(Ni^{II}(SOD-on))$^-$ reaction, both were plotted in Figure 11 (high- vs low-spin Ni^{II} is discussed in the next section).

An inspection of these data suggest another role for the H(1) imidazole in NiSOD besides stabilization of the Ni^{III} oxidation state: ET optimization through redox-potential tunning. As would be expected from the similar values of k_o and λ_{ET}, k_{ET} for the three ET reactions at any given overpotential are similar. However, this does not take into account the different redox potentials for the imidazole ligated versus dissociated Ni-centers. We can estimate the $E_{1/2}$ values from the thin-film voltammetry data displayed in Figure 9. When these differences in overpotential are taken into account there are dramatic differences in k_{ET} for the three calculated redox scenarios. For the O_2 production, reaction the three ET rate constants differ by no more than a factor of 4 ranging between $1.6 \times 10^5\ s^{-1}$ to $6.3 \times 10^5\ s^{-1}$, with the k_{ET} for the imidazole *dissociated* reaction being marginally the fastest. However, at the overpotentials required for H_2O_2 production k_{ET} for the imidazole dissociated reaction is $2.8 \times 10^4\ s^{-1}$ while k_{ET} for the imidazole ligated reaction are $4.6 \times 10^5\ s^{-1}$ and $1.7 \times 10^6\ s^{-1}$. These data imply that for NiSOD, imidazole coordination will shift the $Ni^{II/III}$ redox couple such that it results in an optimization of the driving force at the $O_2^{\bullet-}$ oxidization and reduction overpotentials, and hence a faster Ni-centered redox process.

All of these calculated k_{ET} values are for an outersphere ET process to and from Ni. They therefore are not directly applicable to an innersphere SOD mechanism (i.e., $O_2^{\bullet-}$ coordination to the Ni-center). Such an SOD mechanism may well be taking place in these metallopeptides (and NiSOD), however, CN^- and N_3^- binding studies argue against such a mechanism. We see no evidence that either azide or cyanide anions bind to the Ni^{II}-center of [Ni^{II}(SOD^{M2})] (Supporting Information). Azide does not bind to [Ni^{II}(SOD^{M2})] even when a 300-fold excess of NaN_3 is added to solution. When CN^- (as NaCN) is added to solutions of [Ni^{II}(SOD^{M2})], it completely strips the Ni^{II} ion from the peptide after 4 equiv of NaCN is added to solution (Supporting Information). Furthermore, all available evidence suggests that neither CN^- nor N_3^- binds to the Ni-center of the metalloenzyme NiSOD. Crystallographic studies performed by Getzoff and co-workers demonstrate that neither CN^- nor N_3^- will coordinate to the Ni-center of NiSOD.[14] As we saw with [Ni^{II}(SOD^{M2})], CN^- strips nickel from the active-site of NiSOD. Additionally it was suggested that N_3^- binds to NiSOD in an electrostatic pocket near the Ni-center and does not coordinate to the Ni ion. MCD studies performed by Brunold and co-workers also show that N_3^- does not bind to the Ni^{III} center of NiSOD but near the oxidized Ni-ion.[42] This all strongly suggests that N_3^- and CN^-, and by analogy $O_2^{\bullet-}$, have a very low affinity for the Ni center of NiSOD. This is all evidence in favor of an outersphere redox mechanism for $O_2^{\bullet-}$ disproportionation by both [Ni^{II}(SOD^{M2})] and NiSOD, such as has been proposed for the $O_2^{\bullet-}$ disproportionation mechanism of small molecule MnSOD mimics.[62]

At this time the source of the protons involved in the $O_2^{\bullet-}$ disproportionation mechanism for both our model systems and NiSOD are unknown. In the metalloenzyme the H(1) imidzaole has been largely ruled out as a proton donor since it is far removed from the $O_2^{\bullet-}$ binding pocket, and speculation has focused on Y(9)[14] or a protonated coordinated cysteinate[17,42,63,64] as potential proton donors. In our system there are no major steric limitations, and therefore the imidazole proton could be

(62) Riley, D. P. *Chem. Rev.* **1999**, *99*, 2573−2588.
(63) Szilagyi, R. K.; Bryngelson, P. A.; Maroney, M. J.; Hedman, B.; Hodgson, K. O.; Solomon, E. I. *J. Am. Chem. Soc.* **2004**, *126*, 3018−3019.
(64) Rajeev, P.; Keiji, M.; Djamaladdin, M. *J. Comp. Chem.* **2006**, *27*, 1438−1445.

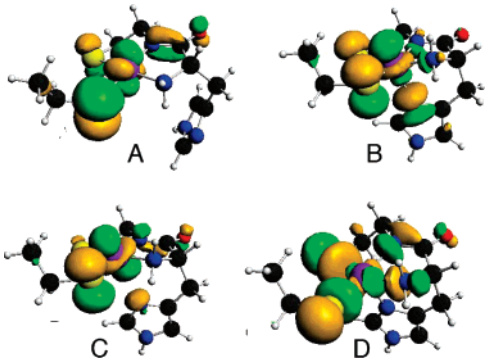

Figure 12. Isosurface plots depicting the HOMOs of $(Ni^{II}(SOD\text{-}off))^-$ (A), $Ni^{III}(SOD\text{-}on)$ (B), $(Ni^{II}(SOD\text{-}on^{l.s.}))^-$ (C), and $(Ni^{II}(SOD\text{-}on^{h.s.}))^-$ (D).

a potential proton donor, as could a number of other potential proton donors contained in the peptide itself as well as bulk water.

High versus Low Spin Ni^{II} in $[Ni^{II}(SOD^{M2})]$. The DFT results from above point to two different possibilities for the spin-state of the five-coordinate Ni^{II} center. Reasonable structures for both triplet, and singlet $(Ni^{II}(SOD\text{-}on))^-$ were obtained. Although high-spin five coordinate Ni^{II} complexes are relatively common, we favor the presence of the low-spin form of five-coordinate $[Ni^{II}(SOD^{M2})]$ during SOD catalysis for a number of reasons. First, the axial Ni−N bond-length (2.618 Å) in $(Ni^{II}(SOD\text{-}on^{l.s.}))^-$ is considerably longer than typically encountered for Ni−N bonds. The structure for the $(Ni^{II}(SOD\text{-}on^{l.s.}))^-$ can therefore be thought of as a square planer Ni^{II} center with an axial Ni^{II}-imidazole *interaction*. Despite the long axial Ni−$N^{imidazole}$ interaction, it does have a significant impact on the electronic structure of the Ni^{II} center.

It has been shown that the HOMO of Ni^{II} contained in square planar N_2S_2 coordination environments is Ni(3d)/S(π)* in character (Figures 12 and 13).[20,42,44,58] Upon "ligation" of the imidazole to the low-spin Ni^{II} center this changes. Although the orbital still has some S(π) character the orbital is now predominately Ni($3d_{z^2}$) in character (Figures 12 and 13; Table 3). Furthermore, the degree of sulfur character in the HOMO significantly decreases from 39.8% in the case of four coordinate $(Ni^{II}(SOD\text{-}off))^-$ to 16.1% in the case of $(Ni^{II}(SOD\text{-}on^{l.s.}))^-$. It has been previously speculated that NiSOD utilizes an anionic amide ligand over a neutral amine-type ligand to avoid potentially destructive S-centered oxidation; utilization of an amide ligand to Ni^{II} (as opposed to an amine ligand) significantly reduces the S character in the HOMO, thus ensuring a Ni-centered redox process.[20,42] Axial imidazole ligation to the low-spin Ni^{II} center further reduces the contribution from the sulfur-based ligands. In addition the redox active molecular orbitals (RAMOs) remain the same when the redox process proceeds from $(Ni^{II}(SOD\text{-}on^{l.s.}))^-$ to $Ni^{III}(SOD\text{-}on)$. In both cases the RAMO is the Ni($3d_{z^2}$)/S(π)* orbital. Also in favor of a singlet ground state is the observation that both $(Ni^{II}(SOD\text{-}on^{l.s.}))^-$ and $Ni^{III}(SOD\text{-}on)$ have their electron density oriented along the *z*-axis, which is the direction of $O_2^{\bullet-}$ attack on the Ni-center. We also note that structural rearrangement between $(Ni^{II}(SOD\text{-}on^{l.s.}))^-$ and $Ni^{III}(SOD\text{-}on)$ is calculated to be facile. In NiSOD a smaller value for λ may be expected because of an elongation of the axial Ni^{III}-His bond by ~0.3 Å relative to these models (both computational and presumably in $[Ni^{III}(SOD^{M2})]$ as well).

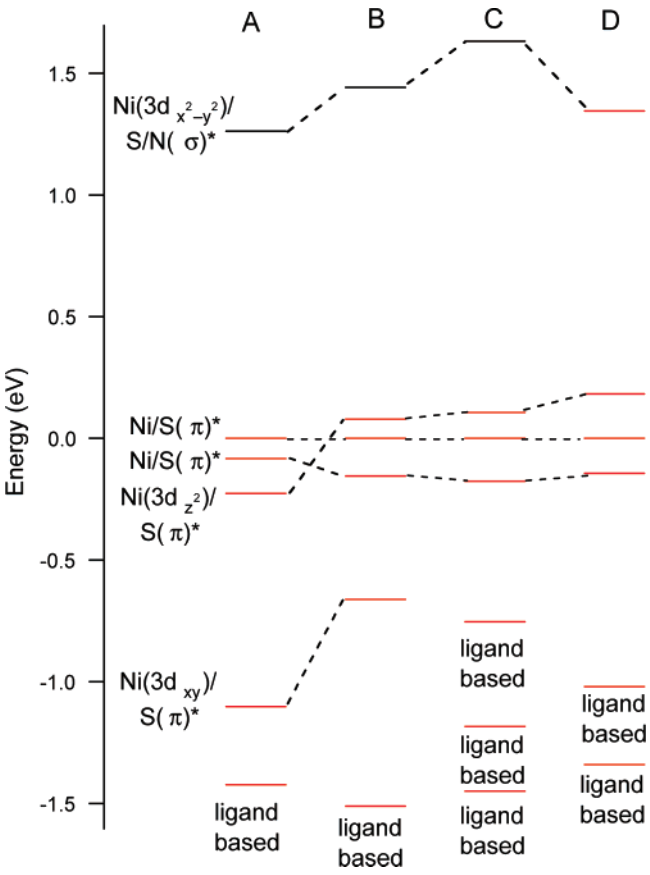

Figure 13. From left to right MO energy diagrams of $(Ni^{II}(SOD\text{-}off))^-$ (A), $(Ni^{II}(SOD\text{-}on^{l.s.}))^-$ (B), $Ni^{III}(SOD\text{-}on)$ (C), and $(Ni^{II}(SOD\text{-}on^{h.s.}))^-$ (D). Energies are all normalized to the highest energy Ni/S(π)* orbital. Occupied MOs are highlighted in red while the unoccupied MOs are in black. For $Ni^{III}(SOD\text{-}on)$ and $(Ni^{II}(SOD\text{-}on^{h.s.}))^-$ the MOs depicted are from the majority spin orbitals.

Table 3. Mulliken Population Analysis[a] of the Ni($3d_{x^2-y^2}$)/N/S(σ)* and Ni($3d_{z^2}$)-S(π)* MOs of $Ni^{II}SOD\text{-}on$, $(Ni^{II}SOD\text{-}on^{l.s.})^-$, and $(Ni^{II}SOD\text{-}on^{h.s.})^-$

	$Ni^{III}SOD\text{-}on$	$(Ni^{II}SOD\text{-}on^{l.s.})^-$	$(Ni^{II}SOD\text{-}on^{h.s.})^-$
Ni($3d_{x^2-y^2}$)/N/S(σ)*	LUMO	LUMO	HOMO
Ni	34.1%	35.0%	34.1%
S	42.7%	30.9%	48.4%
N	12.5%	9.6%	12.5%
Ni($3d_{z^2}$)-S(π)*	HOMO	HOMO	HOMO-1
Ni	32.2%	66.5%	43.1%
S	34.5%	16.1%	52.1%
N	10.7%	2.6%	5.7%

[a] Total percentage of atomic orbital character in the MOs from: Ni 3d/4s/4p, S3 p/3s, N2 p/2s orbitals.

For $(Ni^{II}(SOD\text{-}on^{h.s.}))^-$ the HOMO becomes Ni($3d_{x^2-y^2}$)/N/S(σ)* in character. Thus, the most likely candidate for the RAMO differs in $(Ni^{II}(SOD\text{-}on^{h.s.}))^-$ versus $Ni^{III}(SOD\text{-}on)$. The HOMO also orients electron density along the *x* and *y* axes, away from the direction of $O_2^{\bullet-}$ attack. Furthermore, a relatively large barrier to structural rearrangement is calculated upon going from $(Ni^{II}(SOD\text{-}on^{h.s.}))^-$ to $Ni^{III}(SOD\text{-}on)$, indicating ET may be sluggish between these two species. Finally, we observe that upon conversion from $(Ni^{II}(SOD\text{-}on^{l.s.}))^-$ to $(Ni^{II}(SOD\text{-}on^{h.s.}))^-$ the degree of sulfur character in both the HOMO and HOMO-1 dramatically increases. In both cases the dominate contributer to these MOs in $(Ni^{II}(SOD\text{-}on^{h.s.}))^-$ are the two S-based ligands, resulting in 48.4% S-character in the case of the Ni($3d_{x^2-y^2}$)/

N/S(σ)* HOMO and 52.1% S-character in the Ni($3d_{z^2}$)/S(π)* in the HOMO-1. Thus, a high-spin five coordinate Ni^{II} center in [Ni^{II}(SOD^{M2})] would likely undergo a S-based oxidation process leading to metallopeptide decomposition. Combined these data suggest that a low-spin five-coordinate Ni^{II}-center in [Ni^{II}(SOD^{M2})] during catalysis is physically reasonable.

Summary

The above data suggest that the H(1) imidazole of [Ni-(SOD^{M2})] remains ligated during SOD catalysis. Considering the similarities in the physical properties, structure, and reactivity of the metallopeptide-based model with the metalloenzyme, these data suggest a similar situation is occurring in NiSOD as well. Our metallopeptide based models suggest the axial H(1) imidazole enhances the activity of NiSOD in a number of ways. First, the overall structural rearrangement taking place at the Ni-center is reduced, presumably increasing the rate of the Ni-centered redox processes. Second, the total percentage of S-character in the RAMO of reduced NiSOD is decreased thereby ensuring a Ni-centered oxidation process. Third, the Ni^{II}/Ni^{III} redox potential of the five-coordinate Ni-center would be shifted to a more negative potential relative to a four-coordinate Ni-center such that it would closely match to the midpoint of the $O_2^{\bullet -}$ oxidation and reduction potential.

As a working mechanism (Scheme 1) we propose that starting from the reduced four-coordinate Ni^{II} center NiSOD becomes oxidized to Ni^{III}, and then the H(1) imidazole quickly binds to the Ni^{III} center. Following this the imidazole remains ligated during catalysis. We also suggest that these redox processes takes place through an outersphere ET mechanism between the Ni-center and $O_2^{\bullet -}$. Future studies will be aimed at further refining this mechanism.

Acknowledgment. The University of Nevada, Reno is acknowledged for financial support. XAS data were collected at the NSLS (Brookhaven National Laboratories) under U.S. DOE contract number DEAC02-98CH10886. We are indebted to Dr. A. Dehestani for many helpful discussions.

Supporting Information Available: Glycine titration data, Ni K-edge XAS plots of [Ni^{II}(SOD^{M2}H(1)A)] and [Ni^{II}(SOD^{M2}H-(1)D)], UV−vis spectra of N_3^- and CN^- added to solutions of [Ni^{II}(SOD^{M2})], NBT [Ni^{II}(SOD^{M2}H(1)X)] competition data, and coordinates for the computational models. This material is available free of charge via the Internet at http://pubs.acs.org.

JA0731625